

1 Plateaus and jumps in the atmospheric radiocarbon record – Potential origin and value
2 as global age markers for glacial-to-deglacial paleoceanography, a synthesis

3
4
5 Michael Sarnthein¹⁾, Kevin Küssner²⁾, Pieter M. Grootes³⁾, Blanca Ausin⁴⁾⁸⁾, Timothy
6 Eglinton⁸⁾, Juan Muglia⁵⁾, Raimund Muscheler⁶⁾, Gordon Scholout⁷⁾

7
8
9 1) Institute of Geosciences, University of Kiel, Olshausenstr. 40, 24098 Kiel, Germany,
10 michael.sarnthein@ifg.uni-kiel.de, (corresponding author)

11 2) Alfred-Wegener-Institut Helmholtz-Zentrum für Polar- und Meeresforschung,
12 Department for Marine Geology, 27570 Bremerhaven, Germany, kevin.kuessner@awi.de

13 3) Institute of Ecosystem Research, University of Kiel, Olshausenstr. 40, 24098 Kiel,
14 Germany, pgrootes@ecology.uni-kiel.de

15 4) Geology Department, University of Salamanca, Plaza de los Caldos, 37008
16 Salamanca, Spain, [<ausin@usal.es>](mailto:ausin@usal.es)

17 5) Centro para el Estudio de los Sistemas Marinos, CONICET, 2915 Boulevard Brown,
18 U9120ACD, Puerto Madryn, Argentina, jmuglia@cenpat-conicet.gob.ar

19 6) Quaternary Sciences, Department of Geology Lund University, Sölvegatan 12, 22362
20 Lund, Sweden, raimund.muscheler@geol.lu.se

21 7) Climate Dynamics and Landscape Evolution, GFZ German Centre for Geosciences,
22 Telegrafenberg, 14473 Potsdam, Germany, ScholoutG@gmail.com

23 8) Geological Institute, ETH Zürich, Sonneggstr. 5, 8092 Zuerich, Switzerland,

24
25
26 [final version submitted to CLIMATE OF THE PAST \(2020-7-16\)](#)

27
28

29 ABSTRACT

30 Changes in the geometry of ocean Meridional Overturning Circulation (MOC) are crucial in
31 controlling past changes of climate and the carbon inventory of the atmosphere. However, the
32 accurate timing and global correlation of short-term glacial-to-deglacial changes of MOC in
33 different ocean basins still present a major challenge. The fine structure of jumps and plateaus
34 in atmospheric and planktic radiocarbon (^{14}C) concentration reflects changes in atmospheric ^{14}C
35 production, ocean-atmosphere ^{14}C exchange, and ocean mixing. Plateau boundaries in the
36 atmospheric ^{14}C record of Lake Suigetsu, now tied to Hulu U/Th model-ages instead of optical
37 varve counts, provide a stratigraphic 'rung ladder' of up to 30 age tie points 29 to 10 cal. ka for
38 accurate dating of planktic oceanic ^{14}C records. The age differences between contemporary
39 planktic and atmospheric ^{14}C plateaus record the global distribution of ^{14}C reservoir ages for
40 surface waters of the Last Glacial Maximum (LGM) / deglacial Heinrich Stadial 1 (HS-1), as
41 documented in 19/20 planktic ^{14}C records. Elevated and variable reservoir ages mark both
42 upwelling regions and high-latitude sites covered by sea ice and/or meltwater. ^{14}C ventilation
43 ages of LGM deep waters reveal opposed geometries of Atlantic and Pacific MOC. Like today,
44 Atlantic deep-water formation went along with an estuarine inflow of old abyssal waters from the
45 Southern Ocean up to the northern North Pacific and an outflow of upper deep waters. During
46 early HS-1, ^{14}C ventilation ages suggest a reversed MOC and ~1500 year-long flushing of the
47 deep North Pacific up to the South China Sea, when estuarine circulation geometry marked the
48 North Atlantic, gradually starting near 19 ka. High ^{14}C ventilation ages of LGM deep waters
49 reflect a major drawdown of carbon from the atmosphere. The subsequent major deglacial age
50 drop reflects changes in MOC accompanied by massive carbon releases to the atmosphere as
51 recorded in Antarctic ice cores. These new features of MOC and the carbon cycle provide
52 detailed evidence in space and time to test and refine ocean models that, in part because of
53 insufficient spatial model resolution and reference data, still poorly reproduce our data sets.

54

55

56 1. INTRODUCTION

57 1.1 A variety of terms linked to the notion '¹⁴C age'

58 The ¹⁴C concentration in the troposphere is mainly determined by ¹⁴C production,
59 atmospheric mixing, moreover, air-sea gas exchange and ocean circulation that vary
60 over time (e.g., Alves et al., 2018; Alveson et al., 2018). The ¹⁴C content of living
61 terrestrial plants is in equilibrium with the atmosphere via processes of photosynthesis
62 and respiration. Accordingly, the ¹⁴C of terrestrial plant remains in a sediment section
63 directly reflects the amount of radioactive decay, thus the time passed since the plant's
64 death, and the ¹⁴C composition of the atmosphere during the time of plant growth.

65

66 Contrariwise, ¹⁴C values of marine and inland waters are cut off from cosmogenic ¹⁴C
67 production in the atmosphere, hence depend on the carbon transfer at the air-water
68 interface and the result of local transport and mixing of carbon in the water. For surface
69 waters, the air-sea transfer involves a time span of ten years and less (e.g., Nydal et al.,
70 1998). Yet, vertical and horizontal water mixing results in surface ocean ¹⁴C
71 concentrations on average 5 % lower than those in the contemporaneous atmosphere,
72 a difference expressed as 'Marine Reservoir Age' (or 'reservoir effect' *sensu* Alves et
73 al., 2018). These 'ages' reflect the local oceanography and are highly variable through
74 time (~200–2500 yr; e.g., Stuiver and Braziunas, 1993; Grootes and Sarnthein, 2006;
75 Sarnthein et al., 2015). Apart from U/Th dated corals (many papers on their reservoir
76 age since Adkins and Boyle, 1997), the ¹⁴C age of planktic foraminifers is the most
77 common tracer in marine sediments providing a rough estimate of the time passed
78 since sediment deposition. Soon, however, marine geologists were confronted with age
79 inconsistencies that implied a series of unknowns, in particular the surface ocean ¹⁴C
80 'reservoir age' that finally became a most valuable tracer for oceanography.

81

82 The ^{14}C records of benthic foraminifers in deep-sea sediments reflect the time of
83 radioactive decay since their deposition with the apparent 'ventilation age' of the deep
84 waters in which they lived. Ventilation age is primarily the time span from the moment
85 when carbon dissolved in the local surface waters with somewhat reduced ^{14}C level lost
86 contact with the atmosphere until the precipitation of benthic carbonate from the down-
87 welled deep waters. Details on the derivation of ventilation ages are provided in Cook
88 and Keigwin (2015) and Balmer and Sarnthein (2018). In addition, however, ventilation
89 ages include hardly quantifiable lateral admixtures of older and/or younger water
90 masses, moreover, ^{14}C -enriched organic carbon supplied by the biological pump, thus
91 are called 'apparent'. Today, the apparent transit times of carbon dissolved in the deep
92 ocean range from a few hundred up to ~ 1800 ^{14}C yr found in upper deep waters of the
93 northeastern North Pacific (Matsumoto, 2007).

94

95 The reservoir ages of surface waters and the ventilation ages of deep waters present
96 robust and high-resolution tracers essential for drawing quantitative conclusions on past
97 ocean circulation geometries, marine climate change, and the processes that drive both
98 past ocean dynamics and carbon budgets, given the ages rely on a number of robust
99 age tie points. Obtaining such tie points presents a problem, since any attempt to date a
100 deep-sea sediment record by means of ^{14}C encounters a number of intricacies of how to
101 disentangle the effects of global atmospheric ^{14}C variations due to past changes in
102 cosmogenic ^{14}C production and carbon cycle from (i) local depositional effects such as
103 sediment hiatuses and winnowing, differential bioturbational mixing depth, and sediment
104 transport by deep burrows, (ii) the effects of local atmosphere-ocean exchange and
105 ocean mixing resulting in reservoir and ventilation ages that change through time and

106 space (e.g., Alves et al. 2018; Grootes and Sarnthein, 2006), and (iii) from the final
107 target, quantitatively 'pure' ^{14}C ages due to radioactive decay. These problems are
108 exacerbated by the need for a generally accepted high-precision atmospheric reference
109 record for the period 14–50 cal. ka, beyond tree ring calibration,
110
111 Current ^{14}C -based chronologies of deep-sea sediment records, used to constrain and
112 correlate the age of glacial-to-deglacial changes in ocean dynamics and climate on a
113 global scale, are often of insufficient quality when they are based on (i) age tie points
114 spaced far too wide (e.g., using DO-events 1, 2, and 3 only and/or sporadic tephra
115 layers for the time span 30–14 cal ka), (ii) disregarding atmospheric ^{14}C plateaus, (iii)
116 the risky assumption of \pm constant planktic ^{14}C reservoir ages and other speculative
117 stratigraphic correlations/compilations, and (iv) ignoring small-scale major differences in
118 low-latitude reservoir age. Likewise, clear conclusions are precluded by an uncertainty
119 range of 3-4 kyr sometimes accepted for tie points during the glacial-to-deglacial period
120 (Stern and Lisiecki, 2013; Lisiecki and Stern, 2016), where significant global climate
121 oscillations occurred on decadal-to-centennial time scales as widely shown on the basis
122 of speleothem and ice core-based records (Steffensen et al., 2008; Svensson et al.,
123 2008; Wang et al., 2001). Thus marine paleoclimate and paleoceanographic studies
124 today focus on the continuing quest for a high-resolution and global, hence necessarily
125 atmospheric ^{14}C reference record.

126

127 *1.2 Review of tie points used to fix calibrated and reservoir ages in marine ^{14}C records*

128 The tree ring-based calibration of ^{14}C ages provides a master record of decadal
129 changes in atmospheric ^{14}C concentrations back to ~14 cal. ka (Reimer et al., 2013 and
130 2020) with floating sections beyond (from ~12.5–14.5 cal. ka, around 29–31.5 and 43

131 cal. ka; Turney et al., 2010, 2017, Reimer et al., 2020). The evolution of Holocene and
132 late deglacial ^{14}C ages with time is not linear but reveals variations with numerous
133 distinct jumps (= rapid change) and (short) plateau-shaped (slow or no change or even
134 inversion) structures indicative of fluctuations in atmospheric ^{14}C concentration. Prior to
135 8500 cal. yr BP, various plateaus extend over 400–600 cal. yr and beyond (Fig. 2).
136 Given the quality of the tree ring calibration data, these fluctuations can be considered
137 real, suitable for global correlation (Sarnthein et al., 2007, 2015; Umling and Thunnell,
138 2017; Sarnthein and Werner, 2018). Air-sea gas exchange transfers the atmospheric
139 ^{14}C fluctuations into the surface ocean where they can provide high-resolution tie points
140 to calibrate the marine ^{14}C record and marine reservoir ages back to ~14 ka (via " ^{14}C
141 wiggle matching"). In the near future, however, it is unlikely that a continuous tree ring-
142 based record will become available to trace such atmospheric ^{14}C variations further
143 back, over the period 14–29 cal. ka crucial for the understanding of last-glacial-to-
144 interglacial changes in climate. Hence various other, carbonate-based ^{14}C archives
145 have been employed for this period to reconstruct past changes in atmospheric ^{14}C
146 concentration/age and tie them to an 'absolute' or 'calibrated' (e.g., incremental and/or
147 based on speleothem carbonate) age scale.

148

149 Suites of ^{14}C ages of paired marine and terrestrial plant-borne samples, e.g. paired
150 planktic foraminifers and wood chunks, provide most effective but rarely realizable
151 absolute-age markers and reservoir ages of local ocean surface waters (Zhao and
152 Keigwin, 2018; Rafter et al., 2018; Schroeder et al., 2016; Broecker et al., 2004).
153 Likewise successful appears the alignment of ^{14}C -dated variations in downcore sea-
154 surface temperatures (SST) with changes in hydroclimate as recorded in age-calibrated
155 sedimentary leaf-wax hydrogen isotope (δD) records from ancient lakes (Muschitiello et

156 al., 2019), assumed to be coeval. Further tie points are derived from volcanic ash layers
157 (Waelbroeck et al., 2001; Siani et al., 2013; Davies et al., 2014; Sikes and Guilderson,
158 2016), paired U/Th- and ^{14}C -based coral ages (Adkins and Boyle, 1997; Robinson et al.,
159 2005; Burke and Robinson, 2012; Chen et al., 2015), and the (fairly fragmentary)
160 alignment of major tipping points in ^{14}C dated records of marine SST and planktic $\delta^{18}\text{O}$
161 to the incremental age scale of climate events dated in polar ice core records
162 (Waelbroeck et al., 2011). Such well-defined tie points, however, are wide-spaced in
163 peak glacial-to-early deglacial ice core records, too wide for properly resolving a clear
164 picture of the spatiotemporal pattern of marine paleoclimate events. Finally, various
165 data compilations tentatively rely on the use of multiple age correlations amongst
166 likewise poorly dated marine sediment records, an effort necessarily problematic.
167 Skinner et al. (2019) recently combined new and existing reservoir age estimates from
168 North Atlantic and Southern Ocean to show coherent but distinct regional reservoir age
169 trends in subpolar ocean regions, trends that indeed envelop the range of actual major
170 small-scale and short-term oscillations in reservoir age revealed by our technique of ^{14}C
171 plateau tuning for the subpolar South Pacific (Küssner et al., 2020 subm.).
172
173 Lacking robust age tie points several authors resort to ^{14}C reservoir age simulations for
174 various sea regions by ocean General Circulation Models (GCM) (e.g. Butzin et al.,
175 2017; Muglia et al., 2018) to quantify the potential difference between marine and
176 atmospheric ^{14}C dates for glacial-to-interglacial times. In view of the complexity of ocean
177 MOC and the global carbon cycle it is not surprising that the results of a comparison of
178 a selection of robust empiric vs. simulated ^{14}C reservoir ages are not that encouraging
179 yet (as discussed further below).

180

181 Beyond accepting a generally close link between ^{14}C concentrations in the troposphere
182 and in the surface ocean, the fine structure of planktic ^{14}C records with centennial-scale-
183 resolution can provide a far superior (though costly) link of the marine sediment records
184 to the reference suite of narrow-standing jumps and boundaries of the plateaus robustly
185 identified in the atmospheric ^{14}C record of Lake Suigetsu, the only long, continuous
186 record based on terrestrial plant remains (Bronk Ramsey et al., 2012, 2019). Beyond
187 the reach of the tree ring-based age scale ~ 14 cal. ka, the absolute age of the Suigetsu
188 atmospheric ^{14}C structures can be either calibrated by incremental (microscopy- or
189 XRF-based) varve counts (Scholaut et al., 2018; Marshall et al., 2012) or by a series of
190 paired U/Th- and ^{14}C -based model ages correlated from the Hulu Cave speleothem
191 record (Bronk Ramsey, 2012 and 2019; Southon et al., 2012; Cheng et al., 2018). The
192 difference in absolute age between these calibrations (Fig. 3) is of little importance for
193 the tuning of planktic to corresponding atmospheric ^{14}C plateaus and the derivation of
194 planktic reservoir ages that present the highly variable offset of the ^{14}C age of a planktic
195 plateau from that of the correlated atmospheric plateau. The offset is deduced by
196 subtracting the average ^{14}C age of an atmospheric ^{14}C plateau from that of the
197 correlated planktic ^{14}C plateau, independent of any absolute age value assigned.

198

199 The uncertainty of the Suigetsu atmospheric ^{14}C record is significantly larger than that
200 of the tree ring-based calibration record because of lower ^{14}C concentrations, limited
201 sampling density, and uncertainties in the independent age determination. Thus the ^{14}C
202 fluctuations could be real or represent mere statistical scatter (null hypothesis) in which
203 case the record of atmospheric ^{14}C ages against time would show a simple continuous
204 rise resulting from radioactive decay and the advance of time, such as suggested by a

205 fairly straight progression of the highly resolved deglacial Hulu Cave ^{14}C record plotted
206 vs. U/Th ages (Southon et al., 2012; Cheng et al., 2018).

207

208 The unequivocal fluctuations in the tree ring-based master record of atmospheric ^{14}C
209 concentration (Fig. 2; Reimer et al., 2013, 2020) are on the order of 2–3 % over the last
210 10 kyr (Stuiver and Braziunas, 1993) and even larger back to ~14 ka. Under glacial and
211 deglacial low- CO_2 conditions beyond 14 ka, when climate and ocean dynamics were
212 less constant than during the Holocene, real atmospheric ^{14}C fluctuations were, most
213 likely, even stronger and ^{14}C plateaus and jumps accordingly larger. Plateau-jump
214 structures are also becoming increasingly evident in the evolving atmospheric
215 calibration record (Reimer et al., 2020). The age-defined plateaus and jumps in the
216 Suigetsu atmospheric ^{14}C calibration curve may thus be regarded as a suite of ‘real’
217 structures, extending the calibration provided by the tree ring record for Holocene and
218 B/A-to-Early Holocene times (Fig. 2) into early deglacial and LGM times.

219

220 The plateau/jump structures may partly be linked to changes in cosmogenic ^{14}C
221 production, as possibly shown in the ^{10}Be record (Fig. 4; based on data of Adolphi et al.,
222 2018), and – presumably more dominant – to short-term changes in ocean mixing and
223 the carbon exchange between ocean and atmosphere. The exchange is crucial, since
224 the carbon reservoir of the ocean contains up to 60 (preindustrial) atmospheric carbon
225 units (Berger and Keir, 1984). The apparent contradiction with the smooth Hulu Cave
226 ^{14}C record (Southon et al., 2012; Cheng et al., 2018) may possibly be explained by the
227 Hulu Cave speleothem precipitation system acting as a low-pass filter for fluctuating
228 atmospheric ^{14}C concentrations (statistical tests of Bronk Ramsey et al., pers. comm.
229 2018) and, to a very limited degree, by the obvious scatter in the Suigetsu data. The

230 filter for Hulu data possibly led to a loss especially of short-lived structures in the
231 preserved atmospheric ^{14}C record, though some remainders were preserved in the ^{14}C
232 records of Hulu Cave (Fig. 1). So we rather trust the amplitude of Suigetsu ^{14}C
233 structures than the timing of Hulu Cave data.

234

235 Like a 'rung ladder' the age-calibrated suite of ^{14}C plateau boundaries and jumps is
236 suited for tracing the calibrated age of numerous plateau boundaries in glacial-to-
237 deglacial marine ^{14}C records likewise densely sampled, even when some rungs have
238 been destroyed by local influences on gas exchange or ocean mixing. Also, one may
239 record the average offset of planktic ^{14}C ages from paired atmospheric ^{14}C ages, i.e. the
240 planktic reservoir age, for each single ^{14}C plateau (Sarnthein et al., 2007, 2015). We
241 prefer the Suigetsu record to IntCal, since it is based on original primary atmospheric
242 data and results in small-scale spatio-temporal changes of reservoir age, whereas
243 IntCal is mixing and smoothing a broad array of different data sources with comparativ-
244 ely coarse age resolution, including carbonate-based speleothem and marine records.
245 For the first time, this suite of tie points may facilitate a precise temporal correlation of
246 all sorts of changes in surface and deep-water composition on a global scale, crucial for
247 a better understanding of past changes in ocean and climate dynamics.

248

249 *1.3 Items discussed in this synthesis*

250 The Results Section is summarizing (1) Means to separate noise, global atmospheric
251 and local oceanic forcings that together control the structure of a planktic ^{14}C plateaus,
252 (2) The choice of a U/Th-based reference time scale (Bronk Ramsey et al. 2012; Cheng
253 et al., 2018) instead of the earlier varve-counted version (Schlolut et al., 2018) to date
254 the structures in the global atmospheric ^{14}C record of Lake Suigetsu (Sarnthein et al.,

255 2015), (3) The extension of the suite of age tie points from 23 back to 29 cal. ka, values
256 crucial for an accurate global correlation of ocean events over the Last Glacial
257 Maximum, and (4) Potential linkages of atmospheric ^{14}C plateaus and jumps to
258 cosmogenic ^{14}C production and/or ocean dynamics.

259

260 The Discussion and Implications section includes:

261 (1) A global summary of published marine ^{14}C reservoir age records (Sarnthein et al.
262 2015) now enlarged by nine plateau-tuned records from the Southern Hemisphere
263 (Balmer et al., 2016 and 2018; Küssner et al., 2018 and 2020 subm.) and the northeast
264 Atlantic (Ausin et al., 2020 subm.). In total, 18 (LGM) / 19 (HS-1) plus three wood
265 chunk-based records (Broecker et al., 2004; Zhao et al., 2018) now depict the spatio-
266 temporal variability of past reservoir ages of surface waters in different ocean regions.
267 (2) A comparison of our plateau-based reservoir ages with LGM estimates of surface
268 water ^{14}C reservoir ages simulated by the GCM of Muglia et al. (2018).
269 (3) More detailed insights into the origin of past changes in the global carbon cycle from
270 glacial to interglacial times are provided by the enlarged set of ^{14}C reservoir and venti-
271 lation ages that form a robust tracer of global circulation geometries and the inorganic
272 carbon (DIC) dissolved in different basins of the ocean (Sarnthein et al., 2013).

273

274 The discussion highlights ^{14}C plateau tuning and its revised cal. time scale for global
275 data-model intercomparison and a new understanding of Ocean MOC during the LGM
276 and its reversal during HS-1.

277

278 2. RESULTS – AGE TIE POINTS BASED ON ^{14}C PLATEAU BOUNDARIES

279

280 2.1 *Suite of planktic ¹⁴C plateaus: Means to separate global atmospheric from local*
281 *oceanographic forcings*

282 The basic assumption of the ¹⁴C plateau tuning technique is that the fine structure of
283 fluctuations of the global atmospheric ¹⁴C concentration record can also be found in the
284 surface ocean. In a plot of ¹⁴C age versus calendar age such fluctuations lead to a pattern
285 of plateaus/jumps that correspond to decreases/increases in ¹⁴C concentration. Here we
286 refer to the derivation and interpretation of planktic ¹⁴C plateaus, assuming a predom-
287 inantly global atmospheric origin with occasional local oceanographic forcings. The series
288 of planktic ¹⁴C plateaus and jumps are derived in cores with average hemipelagic
289 sedimentation rates of >10 cm/ky and dating resolution of <100-150 yr. The plateau-
290 specific structures in a sediment age-depth record form a well-defined suite for which
291 absolute age and reservoir age are derived by means of a strict alignment to the reference
292 suite of global atmospheric ¹⁴C plateaus as a whole. Initially, age tie points of planktic
293 foraminiferal $\delta^{18}\text{O}$ records showing (orbital) isotope stages #1-3 serve as stratigraphic
294 guideline for the alignment under the simplifying assumption that stratigraphic gaps are
295 absent, not always true (Suppl. Fig. 2). Planktic reservoir ages and their short-term
296 changes are derived from the difference in average ¹⁴C age between atmosphere and
297 surface waters in subsequent plateaus. To stick as close as possible to the modern range
298 of reservoir ages (Stuiver and Braziunas, 1993), tuned reservoir ages are kept at a
299 minimum unless stringent evidence requires otherwise.

300

301 A close correspondence between ¹⁴C concentrations in atmosphere and surface ocean
302 is expected based on rapid gas exchange. In several cases, however, the specific
303 structure and relative length of a planktic ¹⁴C plateau may deviate from those of the
304 pertinent plateau observed within the suite of atmospheric plateaus, thus indicate local

305 intra-plateau changes of reservoir age. Though less frequent, these changes may indeed
306 amputate and/or deform a plateau, then as result of variations in local ocean atmosphere
307 exchange and oceanic mixing. Two aspects help to sort out short-term climate-driven
308 intra- and inter-plateau changes in ^{14}C reservoir age: (i) The evaluation of the structure
309 and reservoir age of an individual plateau is strictly including the age estimates deduced
310 for the complete suite of plateaus. (ii) Our experience shows that deglacial climate
311 regimes in control of changes in surface ocean dynamics generally occurred on (multi-)
312 millennial time scales (e.g., YD, B/A, HS-1), whereas atmospheric ^{14}C plateaus hardly
313 lasted longer than a few hundred up to 1100 yr (Fig. 1 and S1). Abrupt changes in gas
314 exchange or ocean mixing usually affect one or only a few plateaus of the suite. --
315 Absolute age estimates within a plateau are derived by linear interpolation between the
316 age of the base and top of an undisturbed plateau assuming constant sedimentation
317 rates. The potential impact of short-term sedimentation pulses on ^{14}C plateau formation
318 has largely been discarded by Balmer and Sarnthein (2016).

319

320 *2.2 Suigetsu atmospheric ^{14}C record: Shift to a chronology based on U/Th model ages*

321 Originally, we based the chronology of ^{14}C plateau boundaries in the Suigetsu record
322 (Sarnthein et al., 2015) on a scheme of varve counts by means of light microscopy of
323 thin sections (Bronk Ramsey et al., 2012; Schlolaut et al., 2018). Over the crucial
324 sediment sections of the Last Glacial Maximum (LGM) and deglacial Heinrich Stadial 1
325 (HS-1), however, varve quality / perceptibility in the Suigetsu profile is highly variable
326 (Fig. 5). In parallel, varve-based age estimates were derived from counting various
327 elemental peaks in μXRF data and interpreted as seasonal signals (Marshall et al.,
328 2012). The results obtained from the two independent counting methods and their
329 interpolations widely support each other but diverge for older ages. The varve counts

330 ultimately formed the backbone of a high-resolution chronology obtained by tying the
331 Suigetsu ^{14}C record to the U/Th based time scale of the Hulu cave ^{14}C record (Bronk
332 Ramsey et al., 2012). Recently, Schlolaut et al. (2018) amended the scheme of varve
333 counts. Accordingly, Suigetsu varve preservation (i.e., the number of siderite layers per
334 20 cm thick sediment section) is fairly high prior to ~ 32 ky BP and over late glacial
335 Termination I but fairly poor over large parts of the LGM and HS-1, from $\sim 15 - 32$ cal ka
336 (17.3-28.5 m c.d. in Fig. 5). Here only less than 20-40 % of the annual layers expected
337 from interpolation between clearly varved sections are distinguished by microscopy.
338 Varve counts that use μXRF data (Marshall et al., 2012) can distinguish subtle changes
339 in seasonal element variations, that are not distinguishable in thin section microscopy,
340 hence result in higher varve numbers especially during early deglacial-to-peak glacial
341 times. Yet, some subtle variations are difficult to distinguish from noise, which adds
342 uncertainty to the μXRF -based counts. Thus, the results from either counting method
343 are subject to uncertainties that rise with increased varve age (Fig. 5).

344

345 Bronk Ramsey et al. (2012) established a third time scale based on ^{14}C wiggle matching
346 to U/Th dated ^{14}C records of the Hulu Cave and Bahama speleothems. In part, this
347 calibrated (cal.) age scale was based on Suigetsu varve counts, in part on the
348 prerequisite of the best-possible fit of a pattern of low-frequency changes in ^{14}C
349 concentration obtained from Suigetsu and Hulu Cave. The two ^{14}C records were fitted
350 within the uncertainty envelope of the Hulu 'Old / Dead Carbon Fraction' (OCF/DCF) of
351 ^{14}C concentration. The uncertainty of this model is still incompletely understood. The
352 U/Th-based age model of Suigetsu may suffer from the wiggle matching of atmospheric
353 ^{14}C ages of Lake Suigetsu with ^{14}C ages of the Hulu Cave (Southon et al., 2012) in case
354 of major short-term changes in atmospheric ^{14}C concentration due to a memory effect of

355 soil organic carbon in carbonate-free regions of the cave overburden. The speleothem-
356 carbonate-based Hulu ages may have been influenced far more strongly by short-term
357 changes in the local DCF than assumed, as suggested by major variations in a paired
358 $\delta^{13}\text{C}$ record, that reach up to 5 ‰, mostly subsequent to short-term changes in past
359 monsoon climate (Kong et al., 2005). The uncertainty regarding the assumption of a
360 constant OCF/DCF (Southon et al. 2012; Cheng et al., 2018) may hamper the age
361 model correlation between Hulu and Suigetsu records and the Suigetsu chronology.
362

363 We compared the results of the two timescales, independently deduced from varve
364 counts, with those of the U/Th-based model age scale using as test case the base of
365 ^{14}C Plateau 2b, the oldest tie point constrained by μXRF -based counts. In contrast to
366 16.4 cal. ka, supposed by optical varve counts, μXRF -based counts suggest an age of
367 ~ 16.9 cal. ka (Marshall et al., 2012; Schlolaut et al., 2018), which matches closely the
368 U/Th-based estimate of 16.93 ka. This is a robust argument for the use of the U/Th-
369 based Suigetsu time scale as 'best possible' age scale to calibrate the age of thirty ^{14}C
370 plateau boundaries (Fig. 1). In its older part, the U/Th model time scale is further
371 corroborated by a decent match of short-term increases in ^{14}C concentration with the
372 low geomagnetic intensity of the Mono Lake and Laschamp events at ~ 34 and
373 41.1 ± 0.35 ka (Lascu et al., 2016), independently dated by other methods. The new
374 U/Th-based model ages of ^{14}C plateau boundaries are significantly higher than our
375 earlier microscopy-based varve ages over HS-1 and LGM, a difference increasing from
376 ~ 200 yr near 15.3 cal. ka to ~ 530 near 17 ka and 2000 yr near ~ 29 ka (Fig. 3).

377

378 Note, any readjustment of the calendar age of a ^{14}C plateau boundary does not entail
379 any change in ^{14}C reservoir ages afore deduced for surface waters by means of the

380 plateau technique (Sarnthein et al., 2007, 2015), since each reservoir age presents the
381 simple difference in average ^{14}C age for one and the same ^{14}C plateau likewise defined
382 in both the Suigetsu atmospheric and planktic ^{14}C records of marine surface waters,
383 independent of the precise position of this plateau on the calendar age scale.

384

385 In view of the recent revision of time scales (Schlolut et al., 2018; Bronk Ramsey et al,
386 2019) we now extended our plateau tuning and now also defined the boundaries and
387 age ranges of ^{14}C plateaus and jumps for the interval ~23–29 cal. ka, which results in a
388 total of ~30 atmospheric age tie points for the time span 10.5–29 cal. ka (Fig. 1;
389 summary in Table 1; following the rules of Sarnthein et al., 2007 and 2015). Prior to 25
390 cal. ka, the definition of ^{14}C plateaus somewhat suffered from an enhanced scatter of
391 raw ^{14}C values of Suigetsu. -- In addition to visual inspection, the ^{14}C jumps and
392 plateaus were also defined with higher statistical objectivity by means of the first-
393 derivative of all trends in the ^{14}C age-to-calendar age relationship (or –core depth
394 relationship, respectively) by using a running kernel window (Sarnthein et al., 2015).

395

396 *2.3 Linkages of short-term structures in the atmospheric ^{14}C record to changes in*
397 *cosmogenic ^{14}C production versus changes in ocean dynamics*

398

399 Potential sources of variability in the atmospheric ^{14}C record have first been discussed
400 by Stuiver and coworkers in the context of Holocene fluctuations deduced from tree ring
401 data (e.g., Stuiver and Braziunas 1993), more recently simulated (e.g., Hain et al.,
402 2014). -- Similar to changes in ^{14}C , variations in ^{10}Be deposition in ice cores reflect past
403 changes in ^{10}Be production as a result of changes in solar activity and the strength of
404 the Earth's magnetic field (Adolphi et al., 2018). If we accept to omit assumptions on the

405 modulation of past ^{14}C concentrations by changes in the global carbon cycle we can
406 calculate the atmospheric ^{14}C changes over last glacial-to-deglacial times with ^{10}Be and
407 a carbon cycle model and convert them into ^{14}C ages (Fig. 4). Changes in climate and
408 carbon cycle, however, over this period necessarily modified the ^{10}Be -based ^{14}C record
409 if included correctly into the modeling. Between 10 and 13.5 cal. ka, the ^{10}Be -modeled
410 ^{14}C record displays a number of plateau structures that appear to match the Suigetsu-
411 based atmospheric ^{14}C plateaus. Between 15 and 29 cal. ka, however, ^{10}Be -based ^{14}C
412 plateaus are more rare and/or less pronounced than those in the Suigetsu record. Most
413 modelled plateaus are far shorter than those displayed in the suite of atmospheric ^{14}C
414 plateaus of Lake Suigetsu (e.g., plateaus near to the top 2a, 2b, top 5a, and 9), except
415 for a distinct equivalent of plateau no. 6a. On the whole, the modelled and observed
416 structures show little coherence. This may indicate that any direct relationship between
417 variations in cosmogenic ^{14}C production and the Suigetsu plateau record is largely
418 obscured by the carbon cycle, uncorrected climate effects on the ^{10}Be deposition,
419 and/or noise in the ^{14}C data. Also, a relatively high uncertainty of the measured ^{10}Be
420 concentrations in the ice, (in many cases $\sim 7\%$; Raisbeck et al., 2017), and a lower
421 sample resolution in the order of 50 to 200 yr may contribute to the smoothed character
422 of the ^{10}Be record in Fig. 4.

423

424 On the other hand, the 'new' U/Th-based cal. ages of plateau boundaries may suggest
425 some reasonable stratigraphic correlations between peak glacial and deglacial change in
426 atmospheric CO_2 and ^{14}C plateaus with millennial-scale events in paleoceanography (Fig.
427 6, Table 2): The suite of deglacial ^{14}C plateaus no. 2a, 1, and Top YD indeed displays a
428 temporal match with three brief but major deglacial jumps in ocean degassing of CO_2
429 documented in the WDC ice core (Marcott et al., 2014). The two records have been

430 independently dated by means of annual-layer counts in ice cores and U/Th ages of
431 stalagmites. The match suggests that these atmospheric ^{14}C plateaus may largely result
432 from changes in air-sea gas exchange, and in turn, from changes in ocean dynamics.

433

434 In particular, these events may have been linked to a variety of fast changes such as in
435 sea ice cover in the Southern Ocean and/or in the salinity and buoyancy of high-latitude
436 surface waters (Skinner et al., 2010; Burke and Robinson, 2012). These factors control
437 upwelling and meridional overturning of deep waters, in particular found in the Southern
438 Ocean (Chen et al., 2015) and/or North Pacific (Rae et al. 2014, Gebhardt et al., 2008).
439 Such events of changes in MOC geometry and intensity may be responsible for ocean
440 degassing and the ^{14}C plateaus. The enhanced mixing of the Southern Ocean and a
441 similar, slightly later mixing event in the North Pacific (MD02-2489; Fig. S2d) may have
442 triggered – with phase lag – two trends in parallel, (1) a rise in atmospheric CO_2 , in part
443 abrupt (*sensu* Chen et al., 2015; Menviel et al., 2018), and (2) a gradual enrichment in ^{14}C
444 depleted atmospheric carbon, reflected as ^{14}C plateau.

445

446 Plateau 6a matches a ^{14}C plateau deduced from atmospheric ^{10}Be concentrations, thus
447 suggests changes in ^{14}C production. Other changes in atmospheric ^{14}C (plateaus 4 and
448 8) match short-term North Atlantic warmings during peak glacial and earliest deglacial
449 times, similar to that at the end of HS-1 and during plateau 'YD', hence may reflect
450 minor changes in ocean circulation and ocean-atmosphere exchange without major
451 degassing of old ^{14}C depleted deep waters in the North Atlantic (Table 2, Fig. S2a).

452 There is still little information, however, on the origin of several other peak glacial ^{14}C
453 plateaus 17.5–29 cal. ka. The actual linkages of these plateaus to events in ocean MOC
454 still remain to be uncovered.

455

456 3. DISCUSSION and IMPLICATIONS

457 3.1 ^{14}C plateau boundaries – A suite of narrow-spaced age tie points to rate short-term 458 changes in marine sediment budgets, chemical inventories, and climate 29–10 cal. ka

459

460 In continuation of previous efforts (Sarnthein et al., 2007 and 2015) the tuning of high-
461 resolution planktic ^{14}C records of ocean sediment cores to the new age-calibrated
462 atmospheric ^{14}C plateau boundaries now makes it possible to establish a ‘rung ladder’
463 of ~30 age tie points covering the time span 29 – 10 cal. ka. These global tie points
464 have a time resolution of several hundred to thousand years to be used to constrain the
465 chronology and potential leads and lags of events that occurred during peak glacial and
466 deglacial times (Fig. 1). The locations of 18 (20; depending on the age range covered)
467 ^{14}C records are shown in Fig. 7. Figs. 8 and S2 give the time histories of the planktic
468 and benthic reservoir ages, the information they provide is discussed below.

469

470 Six prominent examples showing the power and value of additional information obtained
471 by means of the ^{14}C plateau-tuning method are:

472 (i) The timing of ocean signals of the onset of deglaciation (sudden depletion of
473 planktic $\delta^{18}\text{O}$ and rise in SST) in the North Atlantic and North Pacific can now be
474 distinguished in detail from those in the Southern Hemisphere, where warming began at
475 17.6 cal. ka, when the cooling of Heinrich 1 started in the North Atlantic (Fig. S2)
476 (Küssner et al., 2020, *subm.*); in harmony with Schmittner and Lund, 2015), a finding
477 important to further constrain global ‘bipolar see-saw’ (Stocker and Johnsen, 2003).

478 (ii) Likewise, the end of the cooling equated with the Antarctic Cold Reversal (ACR;
479 WDC Project Members, 2013) in Pacific surface waters off Central Chile was found

480 precisely coeval with the onset of the Younger Dryas cold spell in the Northern
481 Hemisphere (Küssner et al., 2020, *subm.*).

482 (iii) Signals of local deep-water formation in the subpolar North Pacific can now be
483 separated from signals originating in the North Atlantic (Rae et al. 2014; Sarnthein et al.,
484 2013). In this way we now can specify and tie major short-lasting reversals in Atlantic
485 and Pacific MOC on a global scale.

486 (iv) Signals of deglacial meltwater advection can now be distinguished from short-
487 term interstadial warmings in the northern subtropical Atlantic, which helps to locate
488 meltwater outbreaks far beyond the well-known Heinrich belt of ice-rafted debris
489 (Balmer and Sarnthein, 2018).

490 (v) As outlined above, the timing of marine ^{14}C plateaus can now be compared in
491 detail with that of deglacial events of climate and the atmospheric CO_2 rise independ-
492 ently dated by means of ice core-based stratigraphy (Table 2; Fig. 6). These linkages
493 offer a tool to explore details of deglacial changes in deep-ocean MOC once the suite of
494 ^{14}C plateaus has been properly tuned at any particular ocean site.

495 (vi) The refined scale of age tie points also reveals unexpected details for changes in
496 the sea ice cover of high latitudes as reflected by anomalously high ^{14}C reservoir ages
497 (e.g. north of Iceland and near to the Azores Islands) and for the evolution of Asian
498 summer monsoon in the northern and southern hemisphere as reflected by periods of
499 reduced sea surface salinity (e.g., Sarnthein et al., 2015; Balmer et al., 2018).

500

501 Finally, the plateau-based high-resolution chronology has led to the detection of
502 numerous millennial-scale hiatuses (e.g., Sarnthein et al., 2015; Balmer et al., 2016;
503 Küssner et al., 2020, *subm.*) overlooked by conventional, e.g., *AnalySerie*-based
504 methods (Paillard et al. 1996) of stratigraphic correlation (Fig. S2). In turn, the hiatuses

505 give intriguing new insights into past changes of bottom current dynamics linked to
506 different millennial-scale geometries of overturning circulation and climate change such
507 as in the South China Sea (Sarnthein et al., 2013 and 2015), in the South Atlantic
508 (Balmer et al. 2016) and southern South Pacific (Ronge et al., 2019).

509

510 Clearly, the new atmospheric ^{14}C 'rung ladder' of closely-spaced chronostratigraphic tie
511 points has evolved to a valuable tool to uncover functional chains in paleoceanography,
512 that actually have controlled events of climate change over glacial-to-deglacial times.
513 The extension of the age range back to 29 ka allows constraining potential changes in
514 the ocean dynamics expected for Dansgaard Oeschger (DO) events 2, 3, and 4 as
515 compared to those found for DO-1, though pertinent core records are still missing.

516

517 *3.2 Observed vs. model-based ^{14}C reservoir ages that act as tracer of past changes in*
518 *surface ocean dynamics provide incentive for model refinements*

519

520 Radiocarbon plateau tuning of marine sediment sections to the Suigetsu ^{14}C
521 atmospheric master record allows us to establish at semi-millennial-scale resolution the
522 difference between the average ^{14}C age of coeval atmospheric and planktic ^{14}C
523 plateaus. The suite of changing ^{14}C reservoir ages over time forms a prime tracer of
524 past ocean dynamics influencing local surface waters and a data set crucial to deduce
525 past apparent deep-water ventilation ages (e.g., Muglia et al., 2018; Cook and Keigwin,
526 2015; Balmer and Sarnthein, 2018).

527

528 To better constrain the water depth of past reservoir ages we dated monospecific
529 planktic foraminifera (Sarnthein et al., 2007); in low-to-mid latitudes on *G. bulloides*, *G.*

530 *ruber*, or *G. sacculifer* with habitat depths of 0–80/120 m (Jonkers and Kucera, 2017)
531 and in high latitudes, mostly on *N. pachyderma* (s) living at 0–200 m depth (Simstich et
532 al., 2003). Averaging of ^{14}C ages within a ^{14}C plateau helps to remove analytical noise
533 and minor real ^{14}C fluctuations. Nine plateaus are located in the LGM, 18–27 cal. ka
534 (Fig. 1). Here, planktic foraminifera-based reservoir ages show analytical uncertainties
535 of >200 to >300 yr each for standard AMS dating. By comparison, short-term temporal
536 variations in reservoir age reach 200–400 yr, occasionally up to 600 yr, in particular,
537 close to the end of the LGM (Table 3).

538

539 To better decode the informative value of our ^{14}C reservoir ages for late LGM we
540 compared average ages of ^{14}C Plateaus 4-5 (18.6–20.9 cal. ka) with estimates
541 generated by various global ocean models, an approach similar to that of Toggweiler et
542 al. (2019) applied to modern reservoir ages of the global ocean. In an earlier paper
543 (Balmer et al., 2016) we compared our empiric reservoir ages for the LGM with GCM-
544 based estimates of Franke et al. (2008) and Butzin et al. (2012). Franke et al. (2008)
545 underestimated our mid-latitude values by up to ~ 2000 ^{14}C yr, while LGM reservoir age
546 estimates of Butzin et al. (2012) were more consistent with ours. Their GCM
547 considered more realistic boundary conditions such as the LGM freshwater balance in
548 the Southern Ocean and, in particular, LGM SST and wind fields plus the gas transfer
549 velocity for the exchange of ^{14}C of CO_2 (Sweeney et al., 2007). Further improvements
550 are expected from a model configuration that properly resolves the topographic details
551 of the continental margins and adjacent seas, which frequently form the origin of our
552 sediment-based data sets (Butzin et al., 2020). For the time being, we compared our
553 empirical estimates with estimates from a coarse-resolution GCM, using the results by
554 Muglia et al. (2018; 0–50 m w.d.; Fig. 8c-d; Table 3) as an example. Their model

555 includes ocean surface reservoir age and ocean radiocarbon fields that have been
556 validated through a comparison to LGM ^{14}C data compilation made by Skinner et al.
557 2017. It conforms two plausible, recent model estimates of surface reservoir ages that
558 can be compared to our results (Table 3).

559

560 Low LGM values (300–750 yr) supposedly document an intensive exchange of surface
561 waters with atmospheric CO_2 , most common in model- and foraminifera-based
562 estimates of the low- and mid-latitude Atlantic. Low empiric values also mark LGM
563 waters in mid to high latitudes off Norway and off middle Chile, that is, close to sites of
564 potential deep and/or intermediate water formation. Off Norway and in the northeastern
565 Atlantic, model-based reservoir ages of Muglia et al. (2018) largely match the empiric
566 range. However, the uncertainty envelopes for data shown in Fig. 8c (± 560 yr; $r = 0.59$)
567 generally exceed by far the spatial differences calculated for the empiric data.
568 Conversely, model-based reservoir ages reproduce only poorly the low planktic
569 foraminifera-based estimates off Central Chile and values in the Western Pacific and
570 Southern Ocean.

571 In part, the differences may be linked to problems like insufficient spatial resolution
572 along continental margins, ignoring east-west differences within ocean basins, and/or
573 the estimates of a correct location and extent of seasonal sea ice cover used as LGM
574 boundary condition such as east off Greenland, in the subpolar northwest Pacific, and
575 off Southern Chile, where sea ice hindered the exchange of atmospheric carbon (per
576 analogy to that of temperature exchange, e.g., Sessford et al, 2019). Also, model
577 estimates of the annual average are compared to ^{14}C signals of planktic foraminifera
578 that mostly formed during summer only, e.g., when large parts of the Nordic Seas were

579 found ice-free (Sarnthein et al., 2003). Hence, models may need to better constrain
580 local and seasonal sealing effects of LGM sea ice cover.

581

582 In general, the foraminifera-based reservoir age estimates for our sites that represent
583 various hydrographic key regions in the high-latitude ocean appear much higher than
584 model-derived values. These deviations reach up to 1400 yr, in particular in the
585 Southern Ocean. In part, they may result from the fact that present models may not yet
586 be suited to capture small-scale ocean structures such as the interference of ocean
587 currents with local bathymetry and local upwelling cells. Here, model-based reservoir
588 ages appear far too low in LGM regions influenced by regional upwelling such as the
589 South China Sea then governed by an estuarine overturning system (Wang et al., 2005;
590 Fig. 9), by coastal upwelling off N.W. Australia (Xu et al., 2010; Sarnthein et al., 2011),
591 or by a melt water lid such as off eastern New Zealand (Bostock et al., 2013; Küssner et
592 al., 2020, *subm.*). Local oceanic features are likely to be missed in current resolution
593 models. Our more narrow-spaced empiric data could help to refine the skill of models to
594 capture past ^{14}C reservoir ages.

595

596 Various differences amongst plankton- and model-based reservoir ages may also result
597 from differential seasonal habitats of the different planktic species analyzed that, in turn,
598 may trace different surface and subsurface water currents. Distinct interspecies
599 differences were found in Baja California that record differential, upwelling-controlled
600 habitat conditions (Lindsay et al, 2015). In the northern Norwegian Sea interspecies
601 differences amount up to 600 yr for the Preboreal ^{14}C plateau, 9.6–10.2 cal. ka
602 (Sarnthein and Werner, 2018). Here ^{14}C records of Arctic *Turborotalita quinqueloba*,
603 dominantly grown close to the sea surface during peak summer, differ from the paired

604 record of *Neogloboquadrina pachyderma*, formed in subsurface waters, and that of
605 subpolar species *N. incompta*, mainly advected from the south by Norwegian Current
606 waters well mixed with the atmosphere during peak winter. This makes closer
607 specification of model results as product of different seasonal extremes a further target.

608

609 *3.3 Planktic foraminifera-based ¹⁴C reservoir ages – A prime database to estimate past*
610 *changes in the ¹⁴C ventilation age of deep waters and past oceanic MOC and DIC*

611

612 ‘Raw’ apparent benthic ventilation ages (in ¹⁴C yr; ‘raw’ *sensu* Balmer et al., 2018)
613 express the difference between the (coeval) atmospheric and benthic ¹⁴C levels
614 measured at any site and time of foraminifer deposition. These ages are the sum of (1)
615 the planktic reservoir age of the ¹⁴C plateau that covers a group of paired benthic and
616 planktic ¹⁴C ages and (2) the (positive or negative) ¹⁴C age difference between any
617 benthic ¹⁴C age and the average ¹⁴C age of the paired planktic ¹⁴C plateau. The benthic
618 ventilation ages necessarily rely on the high quality of ¹⁴C plateau-based chronology,
619 since the atmospheric ¹⁴C level has been subject to substantial short-term changes over
620 glacial-to-deglacial times. Necessarily, the ventilation ages include a mixing of different
621 water masses that might originate from different ocean regions and may contribute
622 differential ¹⁴C ventilation ages, an unknown justifying the modifier ‘apparent’.

623

624 In a further step, the $\Delta\Delta^{14}\text{C}$ equivalent of our ‘raw’ benthic ventilation age may be
625 adjusted to changes in atmospheric ¹⁴C that occurred over the (short) time span
626 between deep-water formation and benthic sediment deposition (e.g., Balmer and
627 Sarnthein, 2018; Cook and Keigwin, 2015). In most cases, however, this second step is

628 omitted since its application usually does not imply any major modification of the
629 ventilation age estimates (Fig. S2a; Skinner et al., 2017; Sarnthein et al., 2013).

630

631 On the basis of ^{14}C plateau tuning we now can rely on 18 accurately dated records of
632 apparent benthic ^{14}C ventilation ages (Fig. S2a-d) to reconstruct the global geometry of
633 LGM and HS-1 deep and intermediate water circulation as summarized in ocean
634 transects and maps (Figs. 9–11) and discussed below. The individual matching of our
635 20 planktic ^{14}C plateau sequences with that of the Suigetsu atmospheric ^{14}C record is
636 displayed in Sarnthein et al. (2015), Balmer et al., (2016), Küssner et al. (2020 subm.),
637 and Ausin et al. (in prep.). In addition, robust estimates of past reservoir ages are
638 obtained for 4 planktic and benthic ^{14}C records from paired atmospheric ^{14}C ages of
639 wood chunks (Rafter et al., 2018; Zhao and Keigwin, 2018; Broecker et al., 2004).

640

641 *3.3.1 — Major features of ocean meridional overturning circulation during LGM (Fig. 10)*

642

643 Off Norway and near the Azores Islands very low benthic ^{14}C ventilation ages of <100–
644 750 yr suggest ongoing deep-water formation in the LGM northern North Atlantic
645 reaching down to more than 3000–3500 m water depth, with a flow strength possibly
646 similar to today (and a coeval deep countercurrent of old waters from the Southern
647 Ocean flowing along the East Atlantic continental margin off Portugal). This pattern
648 clearly corroborates the assembled benthic $\delta^{13}\text{C}$ record showing plenty of elevated $\delta^{13}\text{C}$
649 values for the northwestern, eastern and central North Atlantic (Sarnthein et al., 1994;
650 Millo et al., 2006; Keigwin and Swift, 2017). Irrespective of unspecified potential zonal
651 variations in deep-water ventilation age at mid latitudes and different from a number of
652 published models (e.g., Ferrari et al., 2014; Butzin et al., 2017) this ‘anti-estuarine’

653 pattern has been confirmed by MIROC model simulations (Gebbie, 2014; Sherriff-
654 Tadano et al., 2017, Yamamoto et al., 2019) and, independently, by ϵ_{Nd} records (Howe
655 et al., 2016; Lippold et al., 2016). The latter suggest an overturning of AMOC possibly
656 even stronger than today, in particular due to a ‘thermal threshold’ (Abé-Ouchi, pers.
657 comm.) overlooked in other model simulations.

658

659 In contrast to the northern North Atlantic, deep waters in the southern North Atlantic and
660 Circumpolar (CP) deep waters in the subpolar South Atlantic show an LGM ^{14}C
661 ventilation age of ~ 3640 yr, finally rising up to 3800 yr (Figs. 10, 11, S2b). These waters
662 were upwelled and admixed from below to surface waters near to the sub-Antarctic
663 Front during terminal LGM (Fig. S2b; Skinner et al., 2010; Balmer and Sarnthein, 2016;
664 model of Butzin et al., 2012).

665

666 In the southwestern South Pacific abyssal, in part possibly Antarctic-sourced waters
667 (Rae and Broecker, 2018) likewise show high apparent ^{14}C ventilation ages of 3500 yr
668 that drop to 2750 yr near the end of the LGM (Figs. 10 top and S2c) (^{14}C dates of
669 Ronge et al., 2016, modified by planktic ^{14}C reservoir ages of Küssner et al., 2020,
670 *subm.*). A vertical transect of benthic $\delta^{13}C$ (McCave et al., 2008) suggests that the
671 abyssal waters were overlain by CP waters, separated by pronounced stratification near
672 $\sim 3500\text{--}4000$ m water depth. In part, the CP waters stemmed from North Atlantic Deep
673 Water. Probably, their apparent ventilation age 3500 yr came close to the values found
674 in the southern South Atlantic. East of New Zealand the CP waters entered the deep
675 western Pacific and spread up to the subpolar North Pacific, where LGM ^{14}C ventilation
676 ages reached ~ 3700 yr, possibly occasionally 5000 yr (Fig. S2d).

677

678 Similar to today, the MOC of the LGM Pacific was shaped by estuarine geometry,
679 probably more weakened than today (Du et al., 2018) and more distinct in the far
680 northwest than in the far northeast. This geometry resulted in an upwelling of old deep
681 waters in the subarctic Northwest Pacific, here leading to a ^{14}C reservoir age of ~1700
682 yr for surface waters at terminal LGM. On top of the Lower Pacific Deep Waters we may
683 surmise Upper Pacific Deep Waters that moved toward south (Figs. 10 top and 11).

684

685 The Pacific deep waters were overlain by Antarctic / Pacific Intermediate Waters (IW)
686 with LGM ^{14}C ventilation ages as low as 1400–1800 yr, except for a shelf ice-covered
687 site at the southern tip of Chile with IW ages of 2400–2900 yr, possibly a result of local
688 upwelling of CP waters. In general, however, the low values of Pacific IW are similar to
689 those estimated for South Atlantic IW and likewise reflect a vivid exchange with
690 atmospheric CO_2 in their source regions in the Southern Ocean (Skinner et al., 2015).

691

692 When entering and crossing the entrance sill to the marginal South China Sea the
693 ‘young’ IW were mixed with ‘old’ CP waters entrained from below, here leading to ^{14}C
694 ventilation ages of 2600–3450 yr (Figs. 9 and S2d). The LGM South China Sea was
695 shaped by an estuarine-style overturning system marked by major upwelling near to its
696 distal end in the far southwest (Wang L. et al., 1999). This upwelling led to planktic ^{14}C
697 reservoir ages as high as 1200–1800 yr, values rarely found elsewhere in surface
698 waters of low latitudes.

699

700 Our wide-spaced distribution pattern of 18 open-ocean ^{14}C ventilation ages (plus 4
701 values based on paired wood chunks) in Figs. 10 and 11 agrees only in part with the
702 circulation patterns suggested by the much larger datasets of ^{14}C ventilation ages

703 compiled by Skinner et al. (2017) and Zhao et al. (2018). Several features in Figs. 10
704 and 11 directly deviate, e.g., the ages we derive for the North Atlantic and mid-depth
705 Pacific. These deviations may be linked to both the different derivation of our ^{14}C
706 ventilation age estimates and the details of our calendar-year chronology now based on
707 the narrow-standing suite of ^{14}C plateau-boundary ages. The quality of our ^{14}C reservoir
708 ages of surface waters also controls the 'apparent' ventilation age of deep-waters, as it
709 results from direct addition of the short-term average ^{14}C age of a planktic ^{14}C plateau to
710 a paired, that is coeval benthic ^{14}C age (formed during the time of benthic foraminiferal
711 growth, somewhat after the actual time of deep-water formation).

712

713 *3.3.2 — Major features of meridional overturning circulation during early HS-1 (Fig. 10)*

714

715 Near the onset of deglacial Heinrich Stadial 1 (HS-1; ~18–14.7 cal. ka) major shifts in
716 ^{14}C ventilation age suggest some short-lasting but fundamental changes in the
717 circulation geometry of the deep ocean, a central theme of marine paleoclimate
718 research (lower panel of Figs. 10, 11 and S2a and b). Deep waters in the eastern
719 Nordic Seas, west of the Azores Islands, and off northern Brazil show a rapid rise to
720 high ^{14}C ventilation ages of ~2000–2500 yr and up to 4000 yr off Brazil, values that give
721 first proof for a brief switch from 'anti-estuarine' to 'estuarine' circulation that governed
722 the central North Atlantic and Norwegian Sea during early HS-1. This geometry
723 continued – except for a brief but marked and widespread event of recurring NADW
724 formation near 15.2 ka – until the very end of HS-1 near 14.5 ka (Fig. S2a; Muschitiello
725 et al., 2019). The MOC switch from LGM to HS-1 is in line with changes depicted in
726 paired benthic $\delta^{13}\text{C}$ data (Sarnthein et al., 1994), but not confirmed by the coeval ϵ_{Nd}

727 record that suggests a constant source of ‘mid-depth waters’, with the $\delta^{13}\text{C}$ drop being
728 simply linked to a higher age (Howe et al., 2018).

729

730 Conversely, benthic ^{14}C ventilation ages in the northeastern North Pacific (Site MD02-
731 2489) show a coeval and distinct but brief minimum of 1050-1450 yr near 3640 m w.d.
732 during early HS-1 (~18.1–16.8 ka; Figs. 10, 11, and S2d). This minimum was produced
733 by extremely small benthic-planktic age differences of 350–650 yr and provides robust
734 evidence for a millennial-scale event of deep-water formation, that has flushed the
735 northeastern North Pacific down to more than 3640 m w.d. (Gebhardt et al., 2008;
736 Sarnthein et al., 2013; Rae et al., 2014). Similar circulation geometries were reported for
737 the Pliocene (Burls et al., 2017). ‘Young’ Upper North Pacific Deep Waters (North
738 Pacific Intermediate Waters *sensu* Gong et al., 2019) then penetrated as ‘western
739 boundary current’ far south, up to the northern continental margin of the South China
740 Sea (Figs. 9b, 11, and S2d). The short-lasting North Pacific regime of anti-estuarine
741 overturning was similar to that we find in the modern and LGM Atlantic and, most
742 interesting, simultaneous with the Atlantic's estuarine episode.

743

744 Recent data on benthic-planktic ^{14}C age differences (Du et al., 2018) precisely recover
745 our results in a core at ~680 m w.d. off southern Alaska. However, they do not depict
746 the ‘young’ deep waters at their Site U1418 at ~3680 m w.d., as corroborated by a
747 paired autigenic ϵ_{Nd} maximum suggesting a high local bottom water age nearby. We
748 assume that the amazing difference in local deep-water ventilation ages is due to small-
749 scale differences in the effect of Coriolis forcing at high latitudes between a site located
750 directly at the base of the Alaskan continental margin (U1418; Fig. 10b) and that on the
751 distal Murray Sea Mount in the ‘open’ Pacific (MD02-2489; Figs. 7 and 11), which

752 probably has been washed by a plume of newly formed North Pacific deep waters
753 probably stemming from the Bering and/or Ochotsk Seas. In contrast, the incursion of
754 almost 3000 yr old deep waters from the Southern Ocean has continued along the
755 continental margin all over HS-1. In summary we may conclude that the geometry of
756 ocean MOC was briefly reversed in the 'open' North Pacific over almost 1500 years
757 during HS-1, far deeper than suggested by previous authors (e.g., Okazaki et al., 2012;
758 Gong, S., et al. 2019), but similar to changes in geometry first proposed by Broecker et
759 al. (1985) then, however, for an LGM ocean.

760

761 3.3.3 — *Deep-Ocean DIC inventory*

762

763 Apart from the changing geometries in ocean MOC during LGM and HS-1, the global
764 set of ^{14}C plateau-based, hence refined estimates of apparent ^{14}C ventilation ages (Fig.
765 10) has ultimately also revealed new insights into glacial-to-deglacial changes in deep-
766 ocean DIC inventories (Sarnthein et al., 2013; Skinner et al., 2019). On the basis of
767 GLODAP data (Key et al., 2004) any drop in ^{14}C concentration (i.e., any rise in average
768 ^{14}C ventilation age) of modern deep waters is tied linearly to a rise of carbon (DIC)
769 dissolved in deep ocean waters below ~2000 m, making for 1.22 micromole C / -1 ‰
770 ^{14}C . By and large, GCM and box model simulations of Chikamoto and Abé-Ouchi (2012)
771 and Wallmann et al. (2016) suggest that this ratio may also apply to LGM deep-water
772 circulation, when apparent ^{14}C ventilation ages in the Southern Ocean increased
773 significantly (from 2400 up to ~3800 yr) and accordingly, thermohaline circulation was
774 more sluggish and transit times of deep waters extended. Accordingly, a 'back-of-the-
775 envelope' calculation of LGM ventilation age averages in the global deep ocean
776 suggests an additional carbon absorption of 730–980 Gt (Sarnthein et al., 2013). This

777 estimate can easily accommodate the glacial transfer of ~200 Gt C from the atmosphere
778 and biosphere, moreover, may also explain 200–450 Gt C then most probably removed
779 from glacial Atlantic and Pacific intermediate waters. These estimates offer an
780 independent evaluation of ice core-based data, other proxies, and model-based data on
781 past changes in the global carbon cycle (e.g., Menviel et al., 2018).

782

783 4. SOME CONCLUSIONS AND PERSPECTIVES

784 – Despite some analytical scatter, ^{14}C ages for the top and base of Lake Suigetsu-
785 based atmospheric ^{14}C plateaus and coeval planktic ^{14}C plateaus do not present
786 statistical ‘outliers’ but real age estimates that are reproduced by tree ring-based ^{14}C
787 ages over the interval 10–13 cal. ka and further back.

788 – Hulu U/Th model-based ages of ^{14}C plateau boundaries of the Suigetsu atmospheric
789 ^{14}C record appear superior to those derived from microscopy-based varve counts only,
790 since U/Th model-based ages match far more closely the age when now deduced from
791 XRF-based varve counts for the tie point of lower plateau boundary 2b, a test case in
792 the early deglacial, and for the age assigned to the Laschamp event prior to the LGM.

793 – During deglacial times, we show that several atmospheric ^{14}C plateaus paralleled a
794 rise in air-sea gas exchange, and, in turn, distinct changes in ocean MOC. Changes in
795 cosmogenic ^{14}C production rarely provide a complete explanation for the plateaus
796 identified in the Suigetsu ^{14}C data under discussion.

797 – In total, ^{14}C plateau boundaries in the range now provide a suite of ~30 age tie points
798 to establish – like chronological ladder rungs – a robust global age control for deep-sea
799 sediment sections and global stratigraphic correlations of last glacial to deglacial climate
800 events, 29–10 cal. ka. U/Th model ages confine the cal. age uncertainty of Suigetsu
801 plateau boundaries assigned halfway between two ^{14}C ages nearby inside and outside

802 a plateau's scatter band to less than ± 50 to ± 70 yr. Nevertheless, stratigraphic gaps
803 may hamper the accurate tuning of planktic ^{14}C plateaus to their atmospheric
804 equivalents hence result in major discrepancies.

805 – The difference in ^{14}C age between coeval atmospheric and planktic ^{14}C plateaus
806 presents a robust tracer of planktic ^{14}C reservoir ages and shows their high temporal
807 and spatial variability for the LGM and HS-1, now established for 18/20 sediment sites.

808 – Paired reservoir ages obtained from different planktic species document the local
809 distribution patterns of different surface water masses and prevailing foraminiferal
810 habitats at different seasons yet insufficiently considered in model simulations.

811 – New, more robust deep-water ^{14}C ventilation ages, derived on the basis of our robust
812 planktic ^{14}C reservoir ages, reveal geometries of LGM overturning circulation similar to
813 those of today. In contrast, ^{14}C ventilation ages of early HS-1 suggest an almost 1500 yr
814 long event of widely reversed circulation patterns marked by deep-water formation and
815 brief flushing of the northern North Pacific and estuarine circulation geometry in the
816 northern North Atlantic.

817 – Increased glacial ^{14}C ventilation ages and carbon (DIC) inventories of ocean deep
818 waters suggest an LGM drawdown of about 850 Gt C into the deep ocean. Starting with
819 HS-1 a drop of ventilation age suggests carbon released to the atmosphere (Sarnthein
820 et al., 2013).

821 – Site-specific comparison of planktic and model-based reservoir ages estimates
822 highlights the need for further model refinements to make them better reflect the real
823 complex patterns of ocean circulation, including seasonality.

824

825 ACKNOWLEDGMENTS

826 We owe sincere thanks for plenty of stimulations to the 23rd International Radiocarbon
827 Conference in Trondheim, in particular to M-J. Nadeau, and to the IPODS–OC3
828 workshop in Cambridge U.K, 2018, convened by A. Schmittner and L. Skinner.
829 Moreover, we thank for most valuable basic discussions with R. Staff, Glasgow, J.
830 Southon, Irvine CA, and M. Butzin, AWI Bremerhaven, who kindly helped us to discuss
831 the comparison of his model results, and S. Beil, Kiel, for computer assistance. Over the
832 last three years, G. Mollenhauer measured with care hundreds of supplementary ¹⁴C
833 ages in her MICADAS laboratory at AWI Bremerhaven. This study obtained long lasting
834 special support from R. Tiedemann and his colleagues at the AWI Bremerhaven.

835

836 **Author contribution**

837 All authors contributed data and valuable suggestions to write up this synthesis. MS and
838 PG designed the outline of this manuscript. KK, BA, TE and MS provided new marine
839 ¹⁴C records in addition to records previously published. GS displayed the details of
840 Suigetsu varve counts. RM provided a ¹⁰Be-based ¹⁴C record and plots of raw ¹⁴C data
841 sets of Suigetsu und Hulu Cave. Discussions amongst PG, RM, GS and MS served to
842 select U/Th-based model ages as best-possible time scale. JM streamlined the sections
843 on data-model intercomparison.

844

845 **Data availability**

846 Published primary radiocarbon data of all sites are available at PANGAEA de. ¹⁴C data
847 of 5 marine cores still under publication by Küssner et al. (subm.) and Ausin et al.
848 (subm.; also see caption of Fig. S2) are deposited at PANGAEA.

849

850 REFERENCES (99)

851 Adkins, J. F. and Boyle, E. A.: Changing atmospheric $\Delta^{14}\text{C}$ and the record of
852 paleoventilation ages. *Paleoceanography*, 12(3), 337–344, 1997.

853 Adolphi, F., Bronk Ramsey, C., Erhard, T., Lawrence Edwards, R., Cheng, H.,
854 Turney, C.S.M., Cooper, A., Svensson, A., Rasmussen, S.O., Fischer, H., and

855 Muscheler, R.: Connecting the Greenland ice-core and U/Th timescales via cosmogenic
856 radionuclides: testing the synchronicity of Dansgaard–Oeschger events. *Clim. Past*, 14,
857 1755–1781. <https://doi.org/10.5194/cp-14-1755-2018>, 2018.

858 Alves, E.Q., Macario, K., Ascough, P., and Bronk Ramsey, C.: The worldwide
859 marine radiocarbon reservoir effect: definitions, mechanisms, and prospects. *Review of*
860 *Geophysics*, 56, <https://doi.org/10.1002/2017RG000588>, 2018.

861 Alveson, E.Q.: Radiocarbon in the Ocean, *EOS*, 99,
862 <https://doi.org/10.1029/2018EO095429>, 2018.

863 Ausin, B., Haghpor, N., Wacker, L., Voelker, A. H. L., Hodell, D., Magill, C., et al.:
864 Radiocarbon age offsets between two surface dwelling planktonic foraminifera species
865 during abrupt climate events in the SW Iberian margin. *Paleoceanography and*
866 *Paleoclimatology*, 34. <https://doi.org/10.1029/2018PA003490>, 2019.

867 Balmer, S., Sarnthein, M., Mudelsee, M., and Grootes, P. M.: Refined modeling and
868 ^{14}C plateau tuning reveal consistent patterns of glacial and deglacial ^{14}C reservoir ages
869 of surface waters in low-latitude Atlantic. *Paleoceanography*, 31.
870 <https://doi.org/10.1002/2016PA002953>, 2016.

871 Balmer, S. and Sarnthein, M.: Planktic ^{14}C plateaus, a result of short-term
872 sedimentation pulses? – *Radiocarbon*, 58, DOI:10.1017/RDC.2016.100, 11 pp., 2016.

873 Balmer, S. and Sarnthein, M.: Glacial-to deglacial changes in North Atlantic melt-
874 water advection and deep-water formation – Centennial-to-millennial-scale ^{14}C records
875 from the Azores Plateau. *Geochim. Cosmochim. Acta*, 236, 399-415,
876 <https://doi.org/10.1016/j.gca.2018.03.001>, 2018.

877 Berger W.H. and Keir, R.S.: Glacial-Holocene changes in atmospheric CO_2 and the
878 deep-sea record. J.E. Hansen, T. Takahashi (Eds.), *Geophysical Monograph*, 29,
879 American Geophysical Union, Washington, DC, pp. 337–351, 1984.

880 Bostock, H.C., Barrows, T.T., Carter, L., Chase, Z., Cortese, G., et al.: A review of
881 the Australian – New Zealand sector of the Southern Ocean over the last 30 ka (Aus-
882 INTIMATE project). *Quaternary Science Reviews* 74, 35-57, 2013.

883 Broecker W.S, Peteet, D.M., and Rind, D.: Does the ocean-atmosphere system have
884 more than one stable mode of operation? *Nature*, **315**, 21-26, doi:10.1038/315021a0,
885 1985

886 Broecker W.S., Barker, S., Clark, E., Hajdas, I., Bonani, G., and Stott, L.: Ventilation
887 of the Glacial deep Pacific Ocean, *Science*, 306, 1169–1172, 2004.

888 Bronk Ramsey, C., Staff, R. A., Bryant, C. L., Brock, F., Kitagawa, H., van der Plicht,

889 J., Schlolaut, G., Marshall, M. H., Brauer, A., Lamb, H. F., Payne, R. L., Tarasov, P. E.,
890 Haraguchi, T., Gotanda, K., Yonenobu, H., Yokoyama, Y., Tada, R., and Nakagawa, T.:
891 A complete terrestrial radiocarbon record for 11.2 to 52.8 kyr B.P., *Science*, 338, 370–
892 374, 2012.

893 Bronk Ramsey, C. et al., *Radiocarbon*, (in press) 2020.

894 Burke, A. and Robinson, L.F.: The Southern Ocean's role in carbon exchange during
895 the last deglaciation. *Science*, 335, 557-561, 2012.

896 Burls, N.J., Fedorov, A.V., Sigman, D.M., Jaccard, S.L., Tiedemann, R., and Haug,
897 G.H.: Active Pacific meridional overturning circulation (PMOC) during the warm
898 Pliocene. *Sci. Adv.* 2017;3: e1700156, 2017.

899 Butzin, M., Prange, M., Lohmann, G.: Radiocarbon simulations for the glacial ocean:
900 The effects of wind stress, Southern Ocean sea ice and Heinrich events. *Earth Planet.*
901 *Sci. Lett.*, 235, 45-61, 2005.

902 Butzin, M., Prange, M., and Lohmann, G.: Readjustment of glacial radiocarbon
903 chronologies by self-consistent three-dimensional ocean circulation modeling. *Earth*
904 *Planet Sci. Lett.*, 317, 177-184, 2012.

905 Butzin, M., Köhler, P., and Lohmann, G.: Marine radiocarbon reservoir age
906 simulations for the past 50,000 years. *Geophys. Res. Lett.*, 44, 8473–8480,
907 doi:10.1002/2017GL074688, 2017.

908 Butzin, M., Heaton, T.J., Köhler, P., and Lohmann, G.: A short note on marine
909 reservoir age simulations used in INTCAL20. *Radiocarbon*, oo, 1-7, DOI:10.1017/RDC.2020.9,
910 2020.

911 Chen, T., Robinson, L.F., Burke, A., Southon, J., Spooner, P., Morris, P.J., and Ng,
912 H.C.: Synchronous centennial abrupt events in the ocean and atmosphere during the
913 last deglaciation, *Science*, 349, 1537-1541, 2015.

914 Cheng, H., Edwards, R.L., Southon, J., Matsumoto, K., Feinberg, J.M., Sinha, A.,
915 Zhou, W., Li, H., Li, X., Xu, Y., Chen, S., Tan, M., Wang, Q., Wang, Y., and Ning, Y.:
916 Atmospheric $^{14}\text{C}/^{12}\text{C}$ changes during the last glacial period from Hulu Cave, *Science*,
917 362, 1293-1297, 2018.

918 Chikamoto, M.O., Abé-Ouchi, A., Oka, A., Ohgaito, R., and Timmermann, A.:
919 Quantifying the ocean's role in glacial CO_2 reductions, *Climate of the Past*, 8, 545–563,
920 doi:10.5194/cp-8-545-2012, 2012.

921 Cook M.S. and Keigwin L.D.: Radiocarbon profiles of the NW Pacific from the LGM
922 and deglaciation: Evaluating ventilation metrics and the effect of uncertain surface

923 reservoir ages, *Paleoceanography*, 30, 174–195, 2015.

924 Davies, S.M., Davies, P.M., Abbott, Meara, R.H., et al.: A North Atlantic tephro-
925 stratigraphical framework for 130-60 ka b2k: New tephra discoveries, marine based
926 correlations, and future challenges, *Quaternary Science Rev.*, 106, 101-121, 2014.

927 Du, J., Haley, B.A., Mix, A.C., Walczak, M.H., and Praetorius, S.K.: Flushing of the
928 deep Pacific Ocean and the deglacial rise of atmospheric CO₂ concentrations, *Nature*
929 *geoscience*, 11, 749-755, 2018.

930 Ferrari, R., Jansen, M.F., Adkins, J.F., Burke, A., Stewart, A.L., and Thompson, A.F.:
931 Antarctic sea ice control on ocean circulation in present and glacial climates, *Proc.*
932 *National Academy Science*, 111 (24), 8753–8758, 2014.

933 Gebbie, G.: How much did Glacial North Atlantic Water shoal? *Paleoceanography*,
934 29, 190-209, doi:10.1002/2013PA002557, 2014.

935 Gebhardt, H., Sarnthein, M., Kiefer, T., Erlenkeuser, H., Schmieder, F., and Röhl, U.:
936 Paleonutrient and productivity records from the subarctic North Pacific for Pleistocene
937 glacial terminations I to V. *Paleoceanography* 23, PA4212, 1-21,
938 doi:10.1029/2007PA001513, 2008.

939 Gong, S., Lembke-Jene, L., Lohmann, G., Knorr, G., Tiedemann, R., Zou, J.J and
940 Shi, X.F.: Enhanced North Pacific deep-ocean stratification by stronger intermediate
941 water formation during Heinrich Stadial 1. *Nature Communications*, 10: 656.
942 <https://doi.org/10.1038/s41467-019-08606-2>, 2019.

943 Grootes P.M. and Stuiver, M.: Oxygen 18/16 variability in Greenland snow and ice
944 with 1000 to 100000 year time resolution, *J. Geophys. Res.: Oceans* (1978–2012)
945 102(C12), 26455–26470, 1997.

946 Grootes, P.M. and Sarnthein, M.: Marine ¹⁴C reservoir ages oscillate, *PAGES News*,
947 14/3, 18-19, 2006.

948 Hain, M.P., Sigman, D.M., and Haug, G.H.: Distinct roles of the Southern Ocean and
949 North Atlantic in the deglacial atmospheric radiocarbon decline, *Earth Planetary Science*
950 *Letters* 394, 198-208, 2014.

951 Howe, J.N.W., Piotrowski, A.M., Noble, T.L., Mulitza, S., Chiessi, C.M., and Bayon,
952 G.: North Atlantic deep-water production during the last glacial maximum, *Nat.*
953 *Commun.*, 7, 11765, 2016. s

954 Howe, J.N.W., Huang, K-F., Oppo, D.W., Chiessi, C.M., Mulitza, S., Blusztajn, J.,
955 and Piotrowski, A.M.: Similar mid-depth Atlantic water mass provenance during the Last
956 Glacial Maximum and Heinrich Stadial 1, *Earth Planetary Science Letters*, 490, 51-61,

957 2018.

958 Jonkers, L. and Kucera, M.: Quantifying the effect of seasonal and vertical habitat
959 tracking on planktonic foraminifera proxies, *Climate of the Past*, 13, 573-586, 2017.

960 Keigwin, L.D. and Swift, S.A.: Carbon isotope evidence for a northern source of
961 deep water in the glacial western North Atlantic, *PNAS*, 114 (11), 2831-2835, 2017.

962 Key R. M., Kozyr, A., Sabine, C.L., Lee, K., Wanninkhof, R., Bullister, J.L., Feely,
963 R.A., Millero, F.J., Mordy, C., and Peng, T.-H. (2004) A global ocean carbon climat-
964 ology: Results from Global Data Analysis Project (GLODAP), *Global Biogeochem. Cy.*,
965 18, GB4031, doi:10.1029/2004GB002247, 2004.

966 Kong, X., Wang, Y., Wu, J., Cheng, H., Edwards, R.L., and Wang, X.: Complicated
967 responses of stalagmite $\delta^{13}\text{C}$ to climate change during the last glaciation from Hulu
968 Cave, Nanjing, China, *Science in China Ser. D Earth Sciences*, 48, (12), 2174-2181,
969 2005.

970 Küssner, K., Sarnthein, M., Lamy, F., and Tiedemann, R.: High-resolution
971 radiocarbon-based age records trace episodes of *Zoophycos* burrowing, *Marine*
972 *Geology*, 403, 48-56, <http://doi:10.1016/j.margeo.2018.04.01>, 2018.

973 Küssner, K., Sarnthein, M., Lamy, F., Michel, E., Mollenhauer, G., Siani G., and
974 Tiedemann, R.: Glacial-to-deglacial reservoir ages of surface waters in the southern
975 South Pacific, *Paleoc. and Paleoclim.* 30 ms-pp, in prep.).

976 Lascu, I., Feinberg, J.M., Dorale, J.A., Cheng, H., and Edwards, R.L.: Age of the
977 Laschamp excursion determined by U-Th dating of a speleothem geomagnetic record
978 from North America. *Geology*, 44, 139-142, doi:10.1130/G37490.1. 2016

979 Lindsay, C.M., Lehman, S.J., Marchitto, T.M., and Ortiz, J.D.: The surface
980 expression of radiocarbon anomalies near Baja California during deglaciation. *Earth*
981 *Planetary Science Letters*, 422, 67-74, 2015.

982 Lippold, J., Gutjahr, M., Blaser, P., Christner, E., de Cavalho-Fereira, M.L., Mulitza,
983 S. et al.: Deep-water provenance and dynamics of the (de)glacial Atlantic meridional
984 overturning circulation, *Earth Planetary Science Letters*, 445, 68-78, 2016.

985 Lisiecki, L.E. and Stern, J.V.: Regional and global benthic $d^{18}\text{O}$ stacks for the last
986 glacial cycle. *Paleoceanography*, 31, doi:10.1002/2016PA003002, 2016.

987 Löwemark, L. and Grootes, P.M.: Large age differences between planktic
988 foraminifers caused by abundance variations and *Zoophycos* bioturbation,
989 *Paleoceanography*, 19, PA2001, doi:10.1029/2003PA000949, 2004.

990 Marcott, S.A., Bauska, T.K., Buizert, C., Steig, E.J., Rosen, J.L., Cuffey, K.M.,

991 Fudge, T.J., Severinghaus, J.P., Ahn, J., Kalk, M.L., McConnell, J.R., Sowers, T.,
992 Taylor, K.C., White, J.W.C., and Brook, E.J.: Centennial-scale changes in the global
993 carbon cycle during the last deglaciation, *Nature*, 514, 616-619,
994 doi:10.1038/nature13799, 2014.

995 Marshall, M., Schlolaut, G., Brauer, A., Nakagawa, T., Staff, R.A., Bronk Ramsey,
996 C., Lamb, H., Gotanda, K., Haraguchi, T., Yokoyama, Y., Yonenobu, H., Tada, R.,
997 SG06 project members: A novel approach to varve counting using μ XRF and X-
998 radiography in combination with thin-section microscopy, applied to the Late Glacial
999 chronology from Lake Suigetsu, Japan, *Quaternary Geochronology* 13, 70-80, 2012.

1000 McCave, I.N., Carter, I., and Hall, I.R.: Glacial-interglacial changes in water mass
1001 structure and flow in the SW Pacific Ocean, *Quaternary Science Rev.*, 27, 1886–1908,
1002 2008.

1003 Matsumoto, K.: Radiocarbon-based circulation age of the world oceans, *J. Geophys.*
1004 *Res.: Oceans* 112(C9), C09004. <https://doi.org/10.1029/2007JC004095>, 2007.

1005 Menviel, L., Spence, P., Yu, J., Chamberlain, M.A., Matear, R.J., Meissner K.J., and
1006 England, M.H.: Southern Hemisphere westerlies as a driver of the early deglacial
1007 atmospheric CO₂ rise, *Nature communications*, 9:2503, DOI:10.1038/s41467-018-
1008 04876-4, 2018.

1009 Millo, C., Sarnthein, M., and Erlenkeuser, M.: Variability of the Denmark Strait
1010 Overflow during the Last Glacial Maximum, *Boreas*, 35, 50-60, 2006.

1011 Muglia, J., Skinner, L., and Schmittner, A.: Weak overturning circulation and high
1012 Southern Ocean nutrient utilization maximized glacial ocean carbon, *Earth and*
1013 *Planetary Science Letters* 496, 47-56, 2018.

1014 Muschitiello, F., D'Andrea, W.J., Schmittner, A., Heaton, T.J., Balascio, N.L.,
1015 deRoberts, N., Caffee, M.W., Woodruff, T.E., Welten, K.C., Skinner, L.C., Simon, M.H.,
1016 and Dokken T.M.: Deep-water circulation changes lead North Atlantic climate during
1017 deglaciation, *Nature Communications* 10, 1272, doi.org/10.1038/s41467-019-09237-3,
1018 2019.

1019 Naughton, F., Costas, S., Gomes, S.D., Desprat, S., Rodrigues, T., Sanchez Goñi,
1020 M.F., Renssen, H., Trigo, R., Bronk-Ramsey, C., Oliveira, D., Salgueiro, E., Voelker,
1021 A.H.L., and Abrantes, F.: Coupled ocean and atmospheric changes during Greenland
1022 stadial 1 in southwestern Europe, *Quaternary Science Reviews*, 212, 108-120, 2019.

1023 Nydal R., Lovseth K., and Skogseth F. H.: Transfer of bomb ¹⁴C to the ocean
1024 surface, *Radiocarbon* 22(3), 626–635, 1980.

1025 Okazaki, Y., Sagawa, T., Asahi, H., Horikawa, K., and Onodera, J.: Ventilation
1026 changes in the western North Pacific since the last glacial period, *Climate of the Past*, 8,
1027 17-24, doi:10.5194/cp-8-17-2012, 2012.

1028 Paillard, D., Labeyrie, L., and Yiou, P.: Macintosh program performs time-series
1029 analysis, *Eos Trans, AGU*, **77**: 379, 1996.

1030 Rae, J.W.B. and W. Broecker, W.: What fraction of the Pacific and Indian oceans'
1031 deep water is formed in the Southern Ocean? *Biogeosciences*, 15, 3779-3794, 2018.

1032 Rae, J., Sarnthein, M., Foster, G., Ridgwell, A., Grootes, P.M., and Elliott T.: Deep
1033 water formation in the North Pacific and deglacial CO₂ rise, *Paleoceanography*, 29,
1034 doi:10.1002/2013PA002570, 645–667, 2014.

1035 Rafter, P.A., Herguera, J.-C., and Southon, J.R.: Extreme lowering of deglacial
1036 seawater radiocarbon recorded by both epifaunal and infaunal benthic foraminifera in a
1037 wood-dated sediment core, *Climate of the Past* 14, 1977–1989, 2018.

1038 Reimer P.J., Bard, E., Bayliss, A., Beck, J. W., Blackwell, P.G., Bronk Ramsey, C.,
1039 Buck, C.E., Cheng, H., Edwards, R.L., and Friedrich, M.: IntCal13 and Marine13
1040 radiocarbon age calibration curves 0–50,000 years cal. BP, *Radiocarbon* 55, 1869–
1041 1887, 2013.

1042 Reimer, P.J., et al.: The IntCal 20 northern hemisphere radiocarbon calibration curve
1043 (0-55 kcal BP), *Radiocarbon*, 2020 (in press).

1044 Robinson, L.F., Adkins, J.F., Keigwin, L.D., et al.: Radiocarbon variability in the
1045 western North Atlantic during the last deglaciation, *Science*, 310, 1469-1473, 2005.

1046 Ronge, T. A., Tiedemann, R., Lamy, F., et al.: Radiocarbon constraints on the extent
1047 and evolution of the South Pacific glacial carbon pool, *Nature Comm.* 7:11487, 2016.

1048 Ronge, T.A., Sarnthein, M., Roberts, J., Lamy, F., and Tiedemann, R.: East Pacific
1049 Core PS75/059-2: Glacial-to-deglacial stratigraphy revisited, *Paleoceanography and*
1050 *Paleoclimatology*, 34 (4), 432-435, DOI:10.1029/2019PA003569, 2019.

1051 Sarnthein, M., Winn, K., Jung, S.J., Duplessy, J.C., Labeyrie, L., Erlenkeuser, H.,
1052 and Ganssen, G.: Changes in east Atlantic deepwater circulation over the last 30,000
1053 years: eight time slice reconstructions, *Paleoceanography*, 9(2), 209–267, 1994.

1054 Sarnthein, M., Pflaumann, U., and Weinelt, M.: Past extent of sea ice in the northern
1055 North Atlantic inferred from foraminiferal paleotemperature estimates,
1056 *Paleoceanography*, 18(2), 2003.

1057 Sarnthein, M., Grootes, P.M., Kennett, J.P., and Nadeau, M.: ¹⁴C Reservoir ages
1058 show deglacial changes in ocean currents and carbon cycle, *Geophys. Monograph* –

1059 Am. Geophys. Union, 173, 175–196, 2007.

1060 Sarnthein, M., Grootes, P.M., Holbourn, A., Kuhnt, W., and Kühn, H.: Tropical
1061 warming in the Timor Sea led deglacial Antarctic warming and almost coeval
1062 atmospheric CO₂ rise by >500 yr, *Earth Planetary Science Letters*, 302, 337-348, 2011.

1063 Sarnthein, M., Schneider, B., and Grootes, P.M.: Peak glacial 14C ventilation ages
1064 suggest major draw-down of carbon into the abyssal ocean, *Climate of the Past*, 9 (1),
1065 925–965, 2013.

1066 Sarnthein, M., Balmer, S., Grootes, P.M., and Mudelsee, M.: Planktic and benthic
1067 14C reservoir ages for three ocean basins, calibrated by a suite of 14C plateaus in the
1068 glacial-to-deglacial Suigetsu atmospheric 14C record, *Radiocarbon*, 57, 129–151, 2015.

1069 Sarnthein, M. and Werner, K.: Early Holocene planktic foraminifers record species-
1070 specific ¹⁴C reservoir ages in Arctic Gateway, *Marine Micropaleontology*, 135, 45-55.
1071 DOI:10.1016/j.marmicro.2017.07.002, 2018.

1072 Schlolaut, G.: A unique and easy-to-use-tool to deal with incompletely varved
1073 archives 782 – the Varve Interpolation Program 3.0.0, *Quaternary Geochronology*, 2019
1074 (in press).

1075 Schlolaut, G., Staff, R.A., Marshall, M.H., Brauer, A., Bronk Ramsey, C., Lamb, H.F.,
1076 and Nakagawa, T.: Microfacies analysis of the Lake Suigetsu (Japan) sediments from
1077 ~50 to ~10 ka BP and an extended and revised varve based chronology, *Quaternary*
1078 *Science Reviews*, 200, 351-366, 2018.

1079 Schmittner, A. and Lund, D.C.: Early deglacial Atlantic overturning decline and its
1080 role in atmospheric CO₂ rise inferred from carbon isotopes ($\delta^{13}\text{C}$), *Climate of the Past*,
1081 11, 135-152, 2015.

1082 Schroeder, J., Holbourn, A., Küssner, K., and Kuhnt, W.: Hydrological variability in
1083 the southern Makassar Strait during the last glacial termination, *Quaternary Science*
1084 *Reviews*, 154, 143-156, 2016.

1085 Sessford, E.G., Jensen, M.F., Tisserand, A.A., Muschitiello, F., Dokken, T.,
1086 Nisancioglu, K.H., and Jansen, E.: Consistent fluctuations on intermediate water
1087 temperature off the coast off Greenland and Norway during Dansgaard-Oeschger
1088 events, *Quaternary Science Reviews*, 223, 105887, 1-17, 2019.

1089 Sherriff-Tadano, S., Abe-Ouchi, A., Yoshimori, M., Oka, A., and Chan, W.-L.:
1090 (Influence of glacial ice sheets on the Atlantic meridional overturning circulation through
1091 surface wind change, *Climate Dynamics*, 50 (7-8), 2881–2903, 2017.

1092 Siani, G., Michel, E., De Pol-Holz, R., DeVries, T., Lamy, F., Carel, M., Isguder, G.,
1093 Dewilde, F., Lourantou, A.: Carbon isotope records reveal precise timing of enhanced
1094 Southern Ocean upwelling during the last deglaciation, *Nature Communications*, 4,
1095 2758, 2013.

1096 Sikes, E.L. and Guilderson, T.P.: Southwest Pacific Ocean surface reservoir ages
1097 since the last deglaciation: Circulation insights from multiple-core studies. *Paleocean-*
1098 *ography*, 31, 298–310, doi:10.1002/2015PA002855, 2016.

1099 Simstich, J., Sarnthein, M., and Erlenkeuser, H.: Paired $\delta^{18}\text{O}$ signals of
1100 *Neogloboquadrina pachyderma* (s) and *Turborotalita quinqueloba* show thermal
1101 stratification structure in Nordic Seas, *Mar. Micropaleontol.*, 912, 1–19, 2003.

1102 Skinner, L.C., Fallon, S., Waelbroeck, C., Michel, E., and Barker, S.: Ventilation of
1103 the deep Southern Ocean and deglacial CO₂ rise, *Science*, 328, 1147–1151, 2010.

1104 Skinner, L.C., Waelbroeck, C., Scrivner, A.E., and Fallon, S.J.: Radiocarbon
1105 evidence for alternating northern and southern sources of ventilation of the deep
1106 Atlantic carbon pool during the last deglaciation, *PNAS*, 111, 5480–5484, 2014.

1107 Skinner, L.C. *et al.*: Reduced ventilation and enhanced magnitude of the deep
1108 Pacific carbon pool during the last glacial period, *Earth Planetary Science Letters*, **411**,
1109 45-52, 2015.

1110 Skinner, L.C., Primeau, F., Freeman, E., de la Fuente, M., Goodwin, P.A.,
1111 Gottschalk, J., Huang, E., McCave, I.N., Noble, T.L., and Scrivner A.E.: Radiocarbon
1112 constraints on the glacial ocean circulation and its impact on atmospheric CO₂, *Nature*
1113 *communications*, 8:16010, DOI: 10.1038/ncomms16010, 2017.

1114 Skinner, L.C., Muschitiello, F., and Scrivner, A.E.: Marine reservoir age variability
1115 over the last deglaciation: Implications for marine carbon cycling and prospects for
1116 regional radiocarbon calibrations. *Paleoceanography and Paleoclimate*, 34,
1117 doi.org/10.1029/2019PA003667, 2019.

1118 Southon, J., Noronha, A.L., Cheng, H, Edwards, R.L., and Wang, Y.: A high-
1119 resolution record of atmospheric ¹⁴C based on Hulu Cave speleothem H82, *Quaternary*
1120 *Science Reviews*, 33:32-41, 2012.

1121 Steffensen, J.P., Andersen, K.K., Bigler, M., et al.: High-Resolution Greenland Ice
1122 Core Data Show Abrupt Climate Change Happens in Few Years, *Science*, 321, 680;
1123 DOI: 10.1126/science.1157707, 2008.

1124 Stern, J.V. and Lisiecki, L.E.: North Atlantic circulation and reservoir age changes
1125 over the past 41,000 years, *Geophysical Research Letters*, 40, 3693-3697,
1126 doi:10.1002/grl.5067, 2013.

1127 Stocker, T. and Johnsen, S.J.: A minimum thermodynamic model for the bipolar
1128 seesaw, *Paleoceanography*, 18 (4), 1087, doi:10.1029/2003PA000920, 2003.

1129 Stuiver, M. and Braziunas, T.V.: Modeling atmospheric ¹⁴C influences and ¹⁴C ages
1130 of marine samples to 10,000 B.C., *Radiocarbon*, 35, 137–189, 1993.

1131 Svensson, A., Andersen, K.K., Bigler, M., Clausen, H.B., Dahl-Jensen, D., Davies,
1132 S.M., Johnsen, S.J., Muscheler, R., Parrenin, F., Rasmussen, S.O., Röthlisberger, R.,
1133 Seierstad, I., Steffensen, J.P., and Vinther, B.M.: A 60 000 year Greenland stratigraphic
1134 ice core chronology, *Climate of the Past*, 4, 47–57, 2008.

1135 Toggweiler, J.R., Druffel, E.R.M., Key, R.M., and Galbraith, E.D.: Upwelling in the
1136 ocean basins north of the ACC. Part 2: How cool Subantarctic water reaches the
1137 surface in the tropics, *J. Geophysical Research*, DOI:10.1029/2018JC014795, 2019 (in
1138 press).

1139 Turney, C.S.M., Fifield, L.K., Hogg, A.G., et al.: Using New Zealand kauri (*Agathis*
1140 *australis*) to test the synchronicity of abrupt climate change during the Last Glacial
1141 Interval (60,000–11,700 years ago), *Quatern. Sci. Rev.*, 29, 3677–3682, 2010.

1142 Turney, C.S.M., Jones, R.T., Phipps, S.J., et al.: Rapid global ocean-atmosphere
1143 response to Southern Ocean freshening during the last glacial, *Nature communications*,
1144 8:520, doi:10.1038/s41467-017-00577-6, 2017.

1145 Umling, N.E. and Thunell, R.C.: Synchronous deglacial thermocline and deep-
1146 water ventilation in the eastern equatorial Pacific, *Nature communications*, 8, 14203.
1147 DOI: 10.1038/ncomms14203, 2017.

1148 Waelbroeck, C., Duplessy, J.-C., Michel, E., Labeyrie, L., Paillard, D., and Duprat, J.:
1149 The timing of the last deglaciation in North Atlantic climate records, *Nature*, 412, 724–
1150 727, 2001.

1151 Waelbroeck, C., Skinner, L.C., Labeyrie, L., Duplessy, J.-C., Michel, E., Riveiros,
1152 N.V., Gherardi, J.-M., and Dewilde, F.: The timing of deglacial circulation changes in the
1153 Atlantic, *Paleoceanography*, 26, PA3213, <https://doi.org/10.1029/2010PA002007>, 2011.

1154 Wallmann, K., Schneider, B., and Sarthein, M.: Effects of eustatic sea-level
1155 change, ocean dynamics, and nutrient utilization on atmospheric pCO₂ and seawater
1156 composition over the last 130,000 years – a model study, *Climate of the Past*, 12, 339-
1157 375, doi: 10.5194/cp-12-339-2016, 2016.

1158 Wang Y.C, Cheng, H., Edwards, R.L., An, Z.S., Wu, J.Y., Shen, C.-C., and Dorale,
1159 J.A.: A high-resolution absolute-dated Late Pleistocene monsoon record from Hulu
1160 Cave, China, *Science*, 294, 2345-2348. DOI: 10.1126/science.1064618, 2001.

1161 Wang, L.J., Sarnthein, M., Erlenkeuser, H., Grimalt, J., Grootes, P., Heilig, S.,
1162 Ivanova, E., Kienast, M., Pelejero, C., and Pflaumann, U.: East Asian monsoon climate
1163 during the late Pleistocene: High-resolution sediment records from the South China
1164 Sea, *Marine Geology*, 156, 245-284, 1999.

1165 Wang, P., Clemens, S., Beaufort, L., Braconnot, P., Ganssen, G., Jian, Z., Kershaw,
1166 P., and Sarnthein, M.: SCOR/IMAGES Working Group 113 SEAMONS: Evolution and
1167 variability of the Asian Monsoon System: State of the art and outstanding issues,
1168 *Quaternary Science Reviews*, 24 (5-6), 595-629, 2005.

1169 WAIS Divide Project Members: Onset of deglacial warming in West Antarctica driven
1170 by local orbital forcing. *Nature*, 500, 440-444. doi:10.1038/nature12376, 2013.

1171 Xu, J., Kuhnt, W., Holbourn, A., Regenber, M., and Andersen, N.: Indo-Pacific
1172 Warm Pool variability during the Holocene and Last Glacial Maximum, *Paleoceanogr.*,
1173 25, 16, 2010.

1174 Yamamoto, A., Abe-Ouchi, A., Ohgaito, R., Ito, A., and Oka, A.: Glacial CO₂
1175 decrease and deep-water deoxygenation by iron fertilization from glaciogenic dust,
1176 *Climate of the Past*, 15, 981-996.

1177 Yashayaev, I., Seidov, D., and Demirov, E.: A new collective view of oceanography
1178 of the Arctic and North Atlantic basins, *Progress in Oceanography*, 132, 21 pp.,
1179 DOI:<http://dx.doi.org/10.1016/j.pocean.2014.12.012>, 2015.

1180 Zhao, N. and Keigwin, L.D.: An atmospheric chronology for the glacial-deglacial
1181 Eastern Equatorial Pacific, *Nature communications*, 9:3077, DOI:10.1038/s41467-018-
1182 05574-x, 2018.

1183 Zhao, N., Marchal, O., Keigwin, L., Amrhein, D., and Gebbie, G.: A synthesis of
1184 deep-sea radiocarbon records and their (in) consistency with modern ocean ventilation,
1185 *Paleoceanography and Paleoclimatology*, 33, 128-151, 2018.

1186 TABLE CAPTIONS

1187

1188 **Table 1 a and b.** Summary of varve- and U/Th model-based age estimates (Schlolut
 1189 et al., 2018; Bronk Ramsey et al., 2012) for ~30 plateau (pl.) boundaries in the
 1190 atmospheric ¹⁴C record identified in Lake Suigetsu Core SG06₂₀₁₂ by means of visual
 1191 inspection over the interval 10.5–27 cal. ka (Sarnthein et al., 2015, suppl. and modified).
 1192 At the right hand side, three columns give the average (Ø) and uncertainty range of ¹⁴C
 1193 ages for each ¹⁴C plateau.

| SUIGETSU Plateau Top | Depth | Plateau Base | Depth | Ø 14C Age | ±Uncertainty | 14C age BP | | | |
|----------------------|-------------------------|------------------------|-------------------------|------------------------|--------------|---------------|--------------|--------------|-----------------|
| SG06_2012 | (cm c.d.) | (cm c.d.) | (cm c.d.) | of 14C Plateau | (14C yr) | min/max. | | | |
| Plateau no. | Varve-based age (yr BP) | U/Th-based age (yr BP) | Varve-based age (yr BP) | U/Th-based age (yr BP) | (14C yr) | (1.6 σ range) | | | |
| 'Preboreal' | 10525 | 10560 | 1325 | 11100 | 11108 | 1383 | 9525 | -170/+110 | 9356/ 9635 |
| 'Top YD' | 11290 | 11281 | 1402 | 11760 | 11755 | 1453 | 10060 | -100/+35 | 9963/ 10095 |
| 'YD' | 11950 | 11895 | 1467 | 12490 | 12475 | 1525 | 10380 | -170/ 124 | 10211/ 10504 |
| 'no name' | 12885 | 12780 | 1555 | 13160 | 13080 | 1582 | 11000 | -85/ 114 | 10915/ 11114 |
| 1a | 13580 | 13656 | 1626 | 13980 | 14042 | 1657 | 12006 | 100 | 11857/ 12050 |
| 1 | 14095 | 14160 | 1666 | 15095 | 15100 | 1740 | 12471 | 185 | 12315/ 12683 |
| 2a | 15310 | 15420 | 1754 | 16140 | 16520 | 1802 | 13406 | 245 | 13174/ 13665 |
| 2b | 16075 | 16520 | 1802 | 16400 | 16930 | 1820 | 13850 | 40 | 13808/ 13885 |
| 3 | 16835 | 17500 | 1847 | 17500 | 18220 | 1888 | 14671 | 105 | 14582/ 14792 |
| 4 | 17880 | 18650 | 1913 | 18830 | 19590 | 1971 | 15851 | 190 | 15661/ 16044 |

1194

| | | | | | | | | | |
|------------|-------|--------------|------|-------|--------------|------|--------------|-------------|-----------------|
| 5a | 18960 | 19720 | 1978 | 19305 | 20240 | 2003 | 16670 | 90 | 16570/ 16750 |
| 5b | 19305 | 20240 | 2003 | 20000 | 20900 | 2032 | 17007 | 190 | 16830/ 17247 |
| 6a | 20190 | 21000 | 2050 | 20920 | 21890 | 2105 | 17667 | 262 | 17435/ 17960 |
| 6b | 20920 | 21890 | 2105 | 21275 | 22300 | 2132 | 18075 | 140 | 17960/ 18240 |
| 7 | 21375 | 22400 | 2140 | 21790 | 22870 | 2171 | 18843 | 117 | 18741/ 18975 |
| 8 | 21835 | 22940 | 2175 | 22730 | 24250 | 2257 | 19715 | -290 325 | 19425/ 20041 |
| 9 | 22730 | 24250 | 2257 | 23395 | 25150 | 2312 | 20465 | -227 263 | 20238/ 20728 |
| 10a | 23935 | 25880 | 2358 | 25080 | 27000 | 2400 | 22328 | -380 270 | 21946/ 22600 |
| 10b | 25080 | 27000 | 2400 | 25800 | 27600 | 2426 | 22708 | -475 440 | 22233/ 23147 |
| 11 | 26110 | 27770 | 2443 | 27265 | 28730 | 2525 | 24088 | -360 505 | 23727/ 24595 |

1195

1196

1197 **Table 2.** Temporal match of various ¹⁴C plateaus with deglacial periods of major
 1198 atmospheric CO₂ rise and ocean warmings (AA = Antarctic; GIS = Greenland
 1199 Interstadial).

| pCO ₂ RISE (~12 ppm) | Plateau no. | Plateau boundaries |
|--|-------------|--|
| AGE based on annual layers AA ice core (Marcott et al. 2014) | | AGE range (cal. ka) based on U/Th model ages (Bronk Ramsey et al., 2012) |
| 11.7 – 11.5 | # 'Top YD' | 11.83 – 11.3 |
| 14.8 – 14.53 | # 1 | 15.1 – 14.2 |
| 16.4 – 16.15 | # 2a | 16.52 – 15.5 |
| 17.4 – ~17.1 | (data gap) | 17.3 – 17.1 |

FURTHER POTENTIAL CORRELATIVES:

| | | |
|---|--------|----------------------|
| Progressive N. Atlantic warming during the YD at 12.39 – 12.03 ka * | # 'YD' | 12.46 – 11.98 |
| Onset of Antarctic ** warming at 18.3–17.6 ka (ice-based time scale) | #3 | 18.22 – 17.5 |
| Onset of North Atlantic *** warming at 19.3–18.6 ka (U/Th-based time scale) | # 4 | 19.6 – 18.65 |
| Top H2: GIS 2 N. Atlantic warming at 23.4 – 23.3 ka **** | #8 | 24.25 – 22.95 |

AGE CONTROL based on

* Naughton et al. (2019), ** Kawamura et al. (2007),

*** Balmer and Sarnthein (2018), **** Grootes and Stuiver (1997)

1200

1201 **Table 3** a-c. ¹⁴C reservoir / ventilation ages of surface (top 50-100 m) and bottom
 1202 waters vs. U/Th-based model age at 19/22 core sites in the ocean. (a) Spatial and
 1203 temporal changes over early and late LGM (24–21 and 21–18.7 cal. ka), (b) HS-1, and
 1204 the B/A. Late LGM estimates (average res. age of Plateau 4-5) are compared to model-
 1205 based estimates of Muglia et al. (2018). (c) Data sources. For core locations see Fig. 7.
 1206 (a)

| Sediment Core U/Th-based model age Plateau (Pl.) no. | Latitude | Longitude | Water depth (m) | LGM pla. res. age | | LGM model | | res. age | |
|--|----------------------|--------------------|--------------------|---|--|---------------------|--------------|----------|------|
| | | | | 24–21 ka (early LGM) Pl. 8 - 7 - 6 Error (yr) | 21–18.7 ka (late LGM) Pl. 5 - 4 Error (yr) | strong AMOC (yr) | weak (yr) | | |
| ATLANTIC O. | | | | | | | | | |
| PS2644 | 67°52.02'N | 21°45.92'W | 777 | 2100 | ±390 | 1920–2200 | ±325 –±12! | 1136 | 1100 |
| GIK 23074 | 66°66.67'N | 4°90'E | 1157 | 620–790 | ±145–±270 | 550–1175 | ±100–±200 | 1054 | 1059 |
| MD08-3180 | 38°N | 31°13.45'W | 3064 | – | – | 320–605 | ±125–±405 | 827 | 887 |
| SHAK06-5K (= MD99-2334) | 37°34'N (37°48'N) | 10°09'W 10°10'W | 2646 3146 | 675–800 | – | 500–660 | – | 872 | 855 |
| ODP 1002 | 10°42.37'N | 65°10.18'W | 893 | 700–210 | ±230–±310 | 25 – -205 | ±205–±215 | 751 | 738 |
| GeoB 3910-1 | 4°15'S | 36°21'W | 2361 | – | – | – | – | 779 | 796 |
| GeoB 1711-4 | 23°17'S | 12°23'W | 1976 | 1080 | ±290 | 730–840 | ±240–±190 | 711 | 721 |
| KNR 159-5-36GGC | 27°31'S | 46°48'W | 1268 | 540 | ±140 | 870 | ±120 | 757 | 777 |
| MD07-3076 | 44°4'S | 4°12'W | 3770 | – | – | 2300 | ±200 | 928 | 989 |
| INDIAN O./TIMOR SEA | | | | | | | | | |
| MD01-2378 | 13°08.25'S | 121°78.8'E | 1783 | – | – | 2000–1700 | ±300–±320 | 885 | 890 |
| PACIFIC O. | | | | | | | | | |
| MD02-2489 | 54°39.07'N | 148°92.13'W | 3640 | – | – | 1560–1110 | ±310–±335 | 972 | 965 |
| MD01-2416 | 51°26.8'N | 167°72.5'E | 2317 | – | – | 1710 | ±440 | 1227 | 1202 |
| ODP 893A | 34°17.25'N | 120°02.33'W | 588 | – | – | 1065 | ±280 | 839 | 846 |
| MD02-2503 | 34°16.6'N | 120°01.6'W | 580 | – | – | – | – | 839 | 846 |
| GIK 17940 | 20°07.0'N | 117°23.0'E | 1727 | 1820–1260 | ±320–±230 | hiatus | – | 836 | 838 |
| (= SO50-37) | 18°55'N | 115°55'E | 2655 | 1820–1260 | – | – | – | 836 | 840 |
| PS75/104-1 | 44°46'S | 174°31'E | 835 | 1650–1280 | ±210–±320 | 1500 | ±340 | 881 | 895 |
| (= SO213-84) | 45°7.5'S | 174°34,9'E | 972 | 1650–1280 | ±210–±320 | 1500 | ±340 | 881 | 895 |
| MD07-3088 | 46°S | 75°W | 1536 | 385 | ±315 | 380-450 | ±140–±230 | 917 | – |
| SO213-76-2 | 46°13'S | 178°1.7'W | 4339 | – | – | 1460–990 | ±340–±550 | 915 | 842 |
| PS97/137-1 | 52°39.5'S | 75°33.9'E | 1027 | 600–1180 | ±465 | 1180–800 | ±90–±225 | 1505 | 1419 |

1207

1208 (b)

| Sediment Core U/Th-based model age Plateau (Pl.) no. | HS-1 pla. res. age | | 16.5–15.5 ka | | B/A pla. res. age | | LGM be. vent age | | LGM b.w. model age | |
|--|--------------------|------------|--------------|------------|-------------------|------------|------------------|-----------|--------------------|-----------|
| | Pl. 3 - 2b (yr) | Error (yr) | Pl. 2a (yr) | Error (yr) | Pl. 1 - 1a | Error (yr) | early | late | strong AMOC (yr) | weak (yr) |
| ATLANTIC O. | | | | | | | | | | |
| PS2644 | 1775–1660 | ±105–±160 | 1900 | ±355 | – | – | 345 | 2400 | 948 | 918 |
| GIK 23074 | 1730–2000 | ±125–±160 | 670 | ±310 | 140–310 | ±250–±100 | 375 | 375 | 960 | 931 |
| MD08-3180 | 1420–1610 | ±310–±160 | 1460 | ±390 | 630–360 | ±310 | 600 | 600 | 1031 | 1004 |
| SHAK06-5K (= MD99-2334) | 330–410 | – | 535 | – | 780–925 | – | – | 2200–2700 | 1900 | – |
| ODP 1002 | –100 – 20 | ±140 | 90 | ±345 | 355 | ±200 | – | – | 1247 | 1175 |
| GeoB 3910-1 | 630–560 | ±160–±180 | 175 | ±475 | 210–230 | ±220–±110 | 2150 | 2150 | – | – |
| GeoB 1711-4 | 660–690 | ±195–±45 | 420 | ±320 | 880 | ±255 | 1500 | 1500 | 1387 | 1714 |
| KNR 159-5-36GGC | 460–340 | ±380–±300 | 170 | ±700 | 180–230 | ±370–±310 | 1470 | 1470 | 1354 | 1563 |
| MD07-3076 | 1650 | ±180 | – | – | 920 | ±230 | 3640 | 3640 | 1653 | 2060 |
| INDIAN O./TIMOR SEA | | | | | | | | | | |
| MD01-2378 | 740 | ±125 | – | – | 200–185 | ±345–±130 | 2720 | – | 1679 | 1881 |
| PACIFIC O. | | | | | | | | | | |
| MD02-2489 | 800–550 | ±155–±120 | 550 | ±305 | 440 | ±285 | – | 2625 | 2332 | 2595 |
| MD01-2416 | 1480–1140 | ±135–±190 | – | – | 720–570 | ±285–±140 | – | 3700/5100 | 2400 | 2683 |
| ODP 893A | 1065–1490 | ±280–±120 | 1400 | ±370 | 520 | ±185 | – | 1430 | 1677 | 1705 |
| MD02-2503 | 965–1365 | ±160–±160 | 1215 | ±325 | 395–535 | ±240–±130 | – | – | – | – |
| GIK 17940 (= SO50-37) | 1210–1370 | ±200–±470 | 1045 | ±320 | 870–970 | ±325–±100 | 3300–1800 | – | 1807 | 1897 |
| PS75/104-1 (= SO213-84) | 1050 | ±265 | 1180 | ±350 | 800 | ±280 | – | – | – | – |
| MD07-3088 | 800–1090 | ±85–±125 | 1060 | ±275 | 1310–730 | ±125–±190 | 1360 ? | 2400 | 1101 | 1146 |
| SO213-76-2 | 840 | ±310 | – | – | – | – | – | 1500 | 1808 | 1701 |
| PS97/137-1 | 1500–670 | ±90–±180 | 455 | ±270 | – | – | 1400–2400 | 2400/2900 | 1631 | 1871 |

1209

1210 (c)

Sediment Core DATA Source

ATLANTIC O.

| | | |
|----------------------------|--------------------------|----------------|
| PS2644 | Sarnthein et al. 2015 | Be.data suppl. |
| GIK 23074 | Sarnthein et al. 2015 | Be.data suppl. |
| MD08-3180 | Balmer et al. 2018 | |
| SHAK06-5K (= MD99-2334) | Ausin et al., 2020 subm. | |
| ODP 1002 | Skinner et al. 2014 | |
| GeoB 3910-1 | Sarnthein et al. 2015 | |
| GeoB 1711-4 | Balmer et al. 2016 | |
| KNR 159-5-36GGC | Balmer et al. 2016 | data suppl. |
| MD07-3076 | Balmer et al. 2016 | |

INDIAN O./TIMOR SEA

| | | |
|-----------|-----------------------|--|
| MD01-2378 | Sarnthein et al. 2015 | |
|-----------|-----------------------|--|

PACIFIC O.

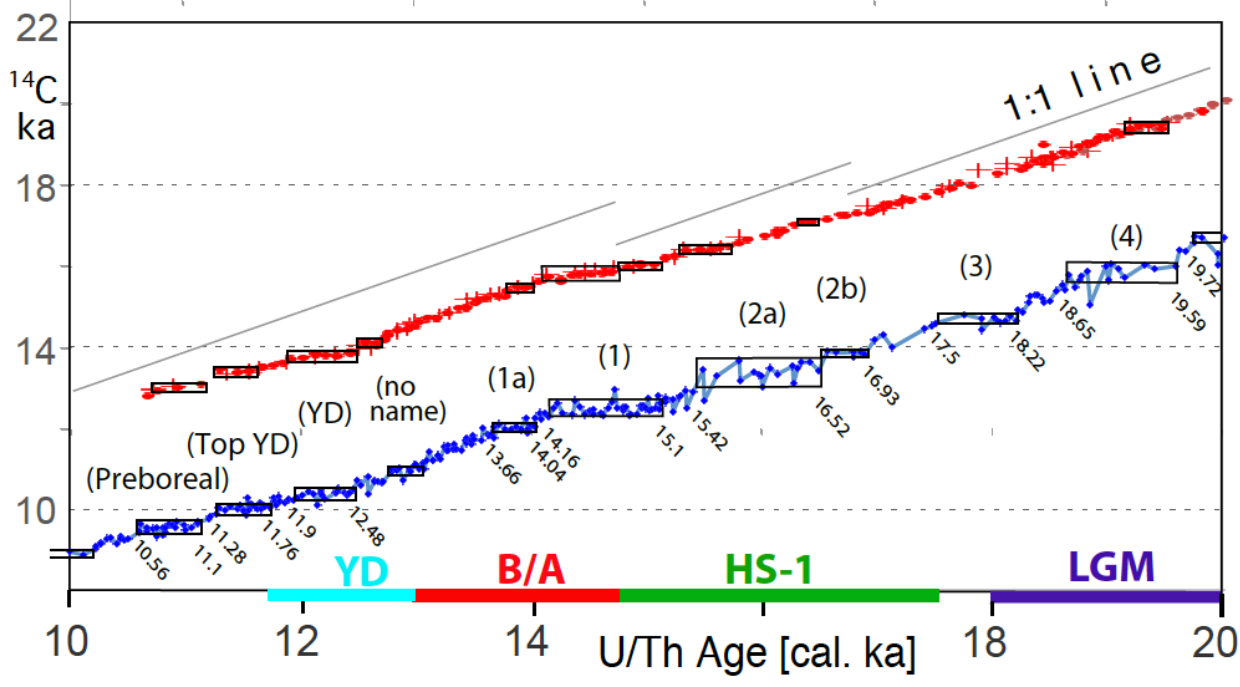
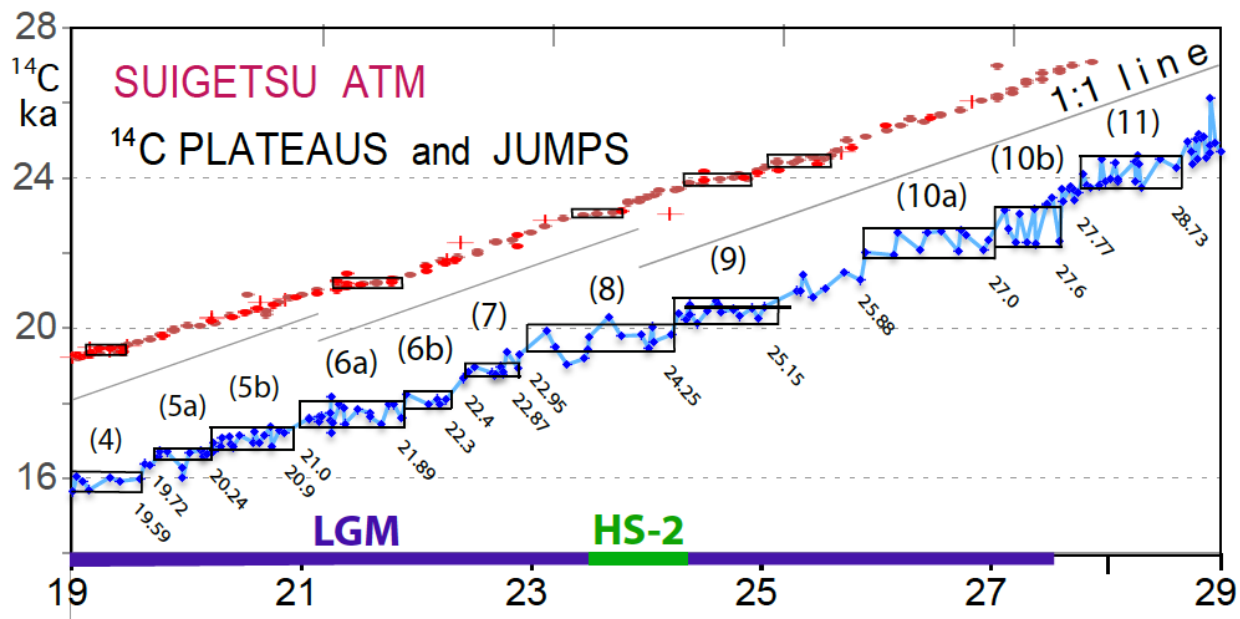
| | | |
|----------------------------|---------------------------|-------------------|
| MD02-2489 | Sarnthein et al. 2015 | |
| MD01-2416 | Sarnthein et al. 2015 | modified |
| ODP 893A | Sarnthein et al. 2015 | data suppl. |
| MD02-2503 | Sarnthein et al. 2015 | |
| GIK 17940 (= SO50-37) | Sarnthein et al. 2015 | |
| PS75/104-1 (= SO213-84) | Sarnthein et al. 2015 | |
| MD07-3088 | Küssner et al., 2020 subm | Siani et al. 2013 |
| SO213-76-2 | Küssner et al., 2020 subm | Ronge et al. 2016 |
| PS97/137-1 | Küssner et al., 2020 subm | data suppl. |

1211 (c)

1212 FIGURE CAPTIONS

1213

1214 – Fig. 1. Atmospheric ^{14}C ages of Lake Suigetsu plant macrofossils 10–20 cal. ka
1215 (bottom panel) and 19–29 cal. ka (top panel) vs. U/Th-based model age (blue dots;
1216 Bronk Ramsey et al., 2012). The 1:1 line reflects gradient of one ^{14}C yr / cal. yr. Double
1217 and triple ^{14}C measurements are averaged. (In part large) error bars of single ^{14}C ages
1218 are given in Suppl. Fig. S1. Suite of labeled horizontal boxes that envelop scatter bands
1219 of largely constant ^{14}C ages shows ^{14}C plateaus longer than 250 yr (plateau boundary
1220 ages listed in Table 1). Red and brown dots (powder samples from trench and wall) and
1221 + signs (off-axis samples) depict raw ^{14}C ages of Hulu stalagmites H82 and MSD
1222 (Cheng et al., 2018; Southon et al., 2012; plot offset by +3000 ^{14}C yr). Suite of short ^{14}C
1223 plateaus (black boxes) tentatively assigned to Hulu-based record occupies age ranges
1224 slightly different from those deduced for Suigetsu-based plateaus. The difference
1225 possibly results from short-term changes in the Old / Dead Carbon Fraction (ocf / dcf)
1226 that in turn may reflect major short-term changes in LGM and deglacial monsoon
1227 climate (Wang et al., 2001; Kong et al., 2005).

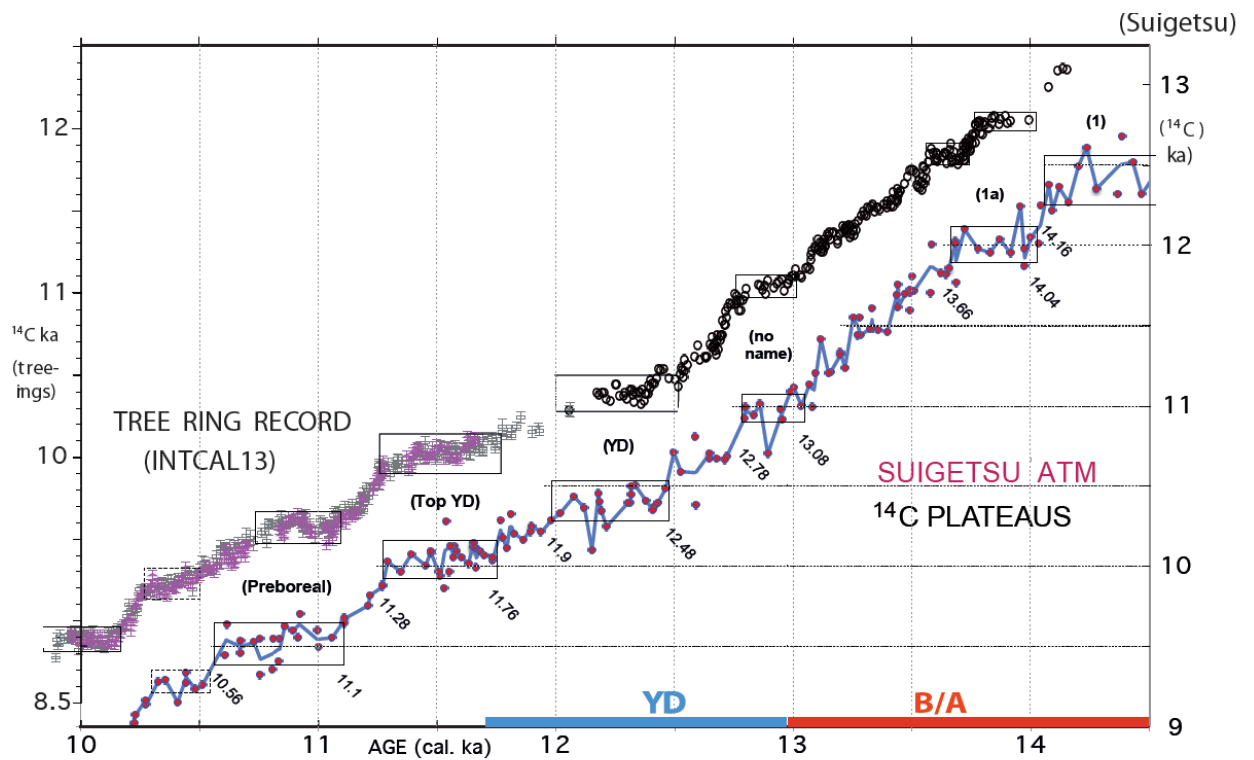


1228

1229

1230

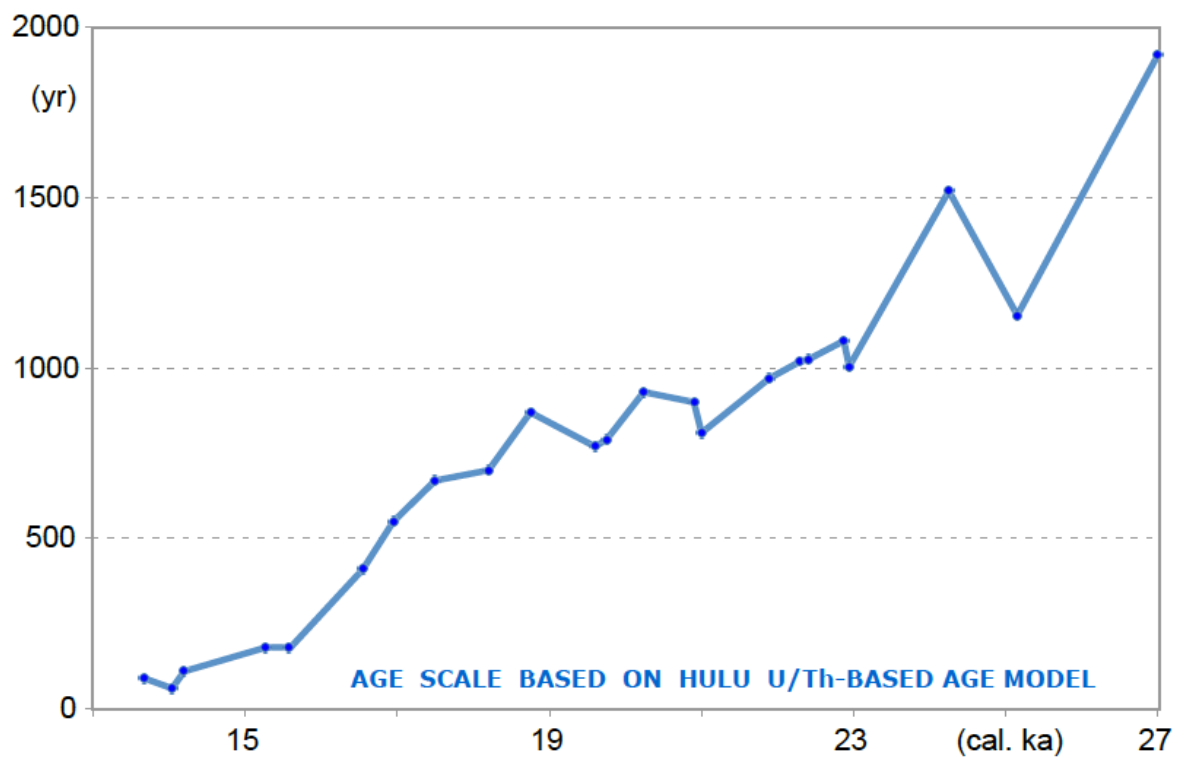
1231 ✗ Fig. 2. High-resolution record of atmospheric ^{14}C jumps and plateaus (= suite of
 1232 labeled horizontal boxes that envelop scatter bands of largely constant ^{14}C ages
 1233 extending over >300 cal. yr) in a sediment section of Lake Suigetsu vs. tree ring-based
 1234 ^{14}C jumps and plateaus 10–14.5 cal. ka (Reimer et al., 2013). Blue line averages paired
 1235 double and triple ^{14}C ages of Suigetsu plant macrofossils. Age control points (cal. ka)
 1236 follow varve counts (Scholaut et al., 2018) and U/Th model-based ages of Bronk
 1237 Ramsey et al. (2012). YD = Younger Dryas, B/A = Bølling-Allerød.
 1238



1239
 1240
 1241
 1242
 1243
 1244
 1245
 1246
 1247
 1248
 1249

1250 ✖ Fig. 3. Difference between Hulu Cave U/Th-based model ages (Southon et al., 2012;
1251 Bronk Ramsey et al., 2012; Cheng et al., 2018) and varve count-based cal. ages for
1252 atmospheric ¹⁴C plateau boundaries in Lake Suigetsu sediment record (Schlolut et al.,
1253 2018) (Sarnthein et al., 2015, suppl. and revised), displayed on the U/Th-based time
1254 scale 13–27 cal. ka.

1255



1256

1257

1258

1259

1260

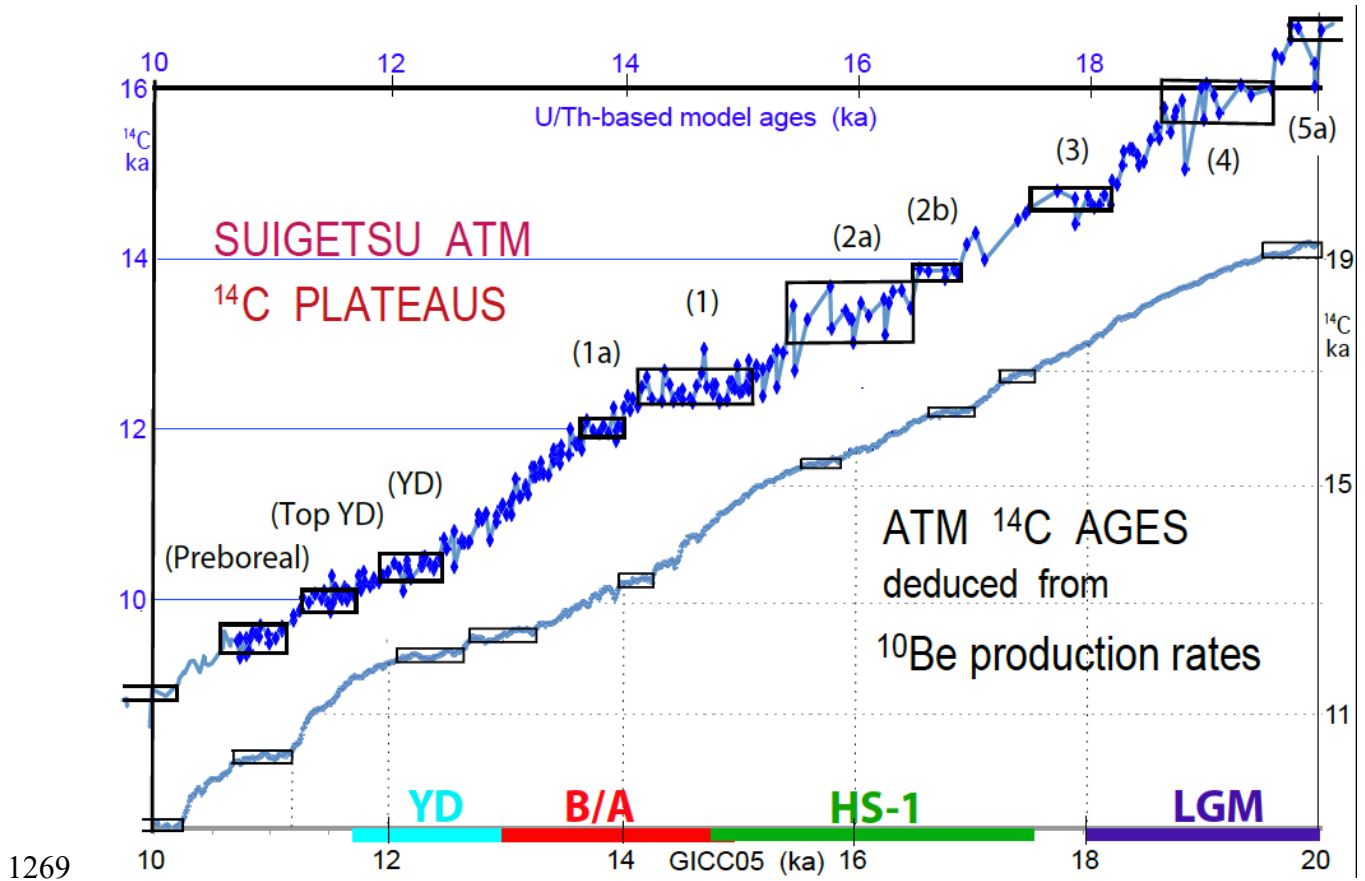
1261

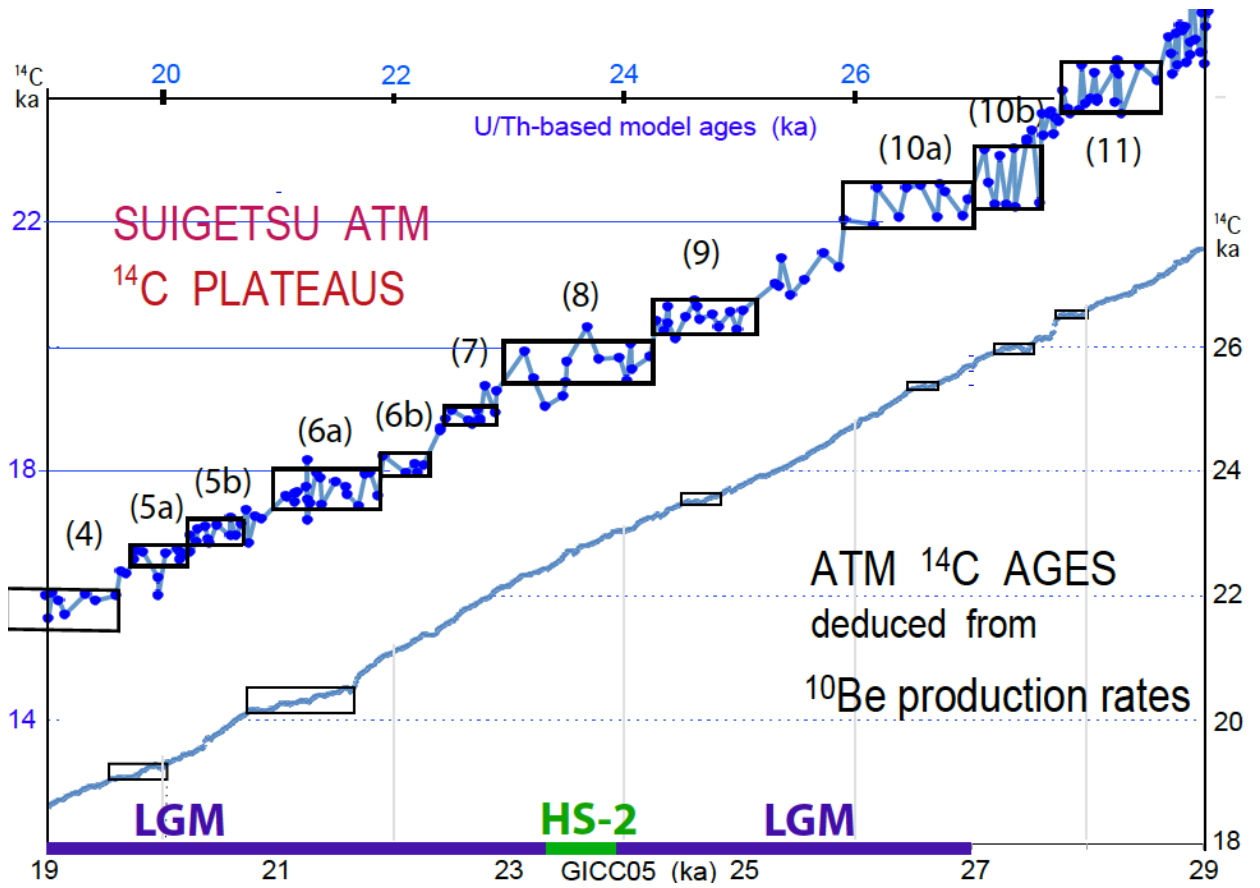
1262

1263

1264

1265 √ Fig. 4 a and b. Atmospheric ^{14}C ages and plateaus (horizontal boxes) deduced from
 1266 ^{10}Be production rates vs. GICC05 age scale (Adolphi et al., 2018) compared to the
 1267 Suigetsu record of atmospheric ^{14}C plateaus vs. Hulu U/Th-based model ages (Southon
 1268 et al., 2012; Cheng et al., 2018) for the intervals a) 10-20 and b) 19-29 cal ka BP.





1270

1271

1272

1273

1274

1275

1276

1277

1278

1279

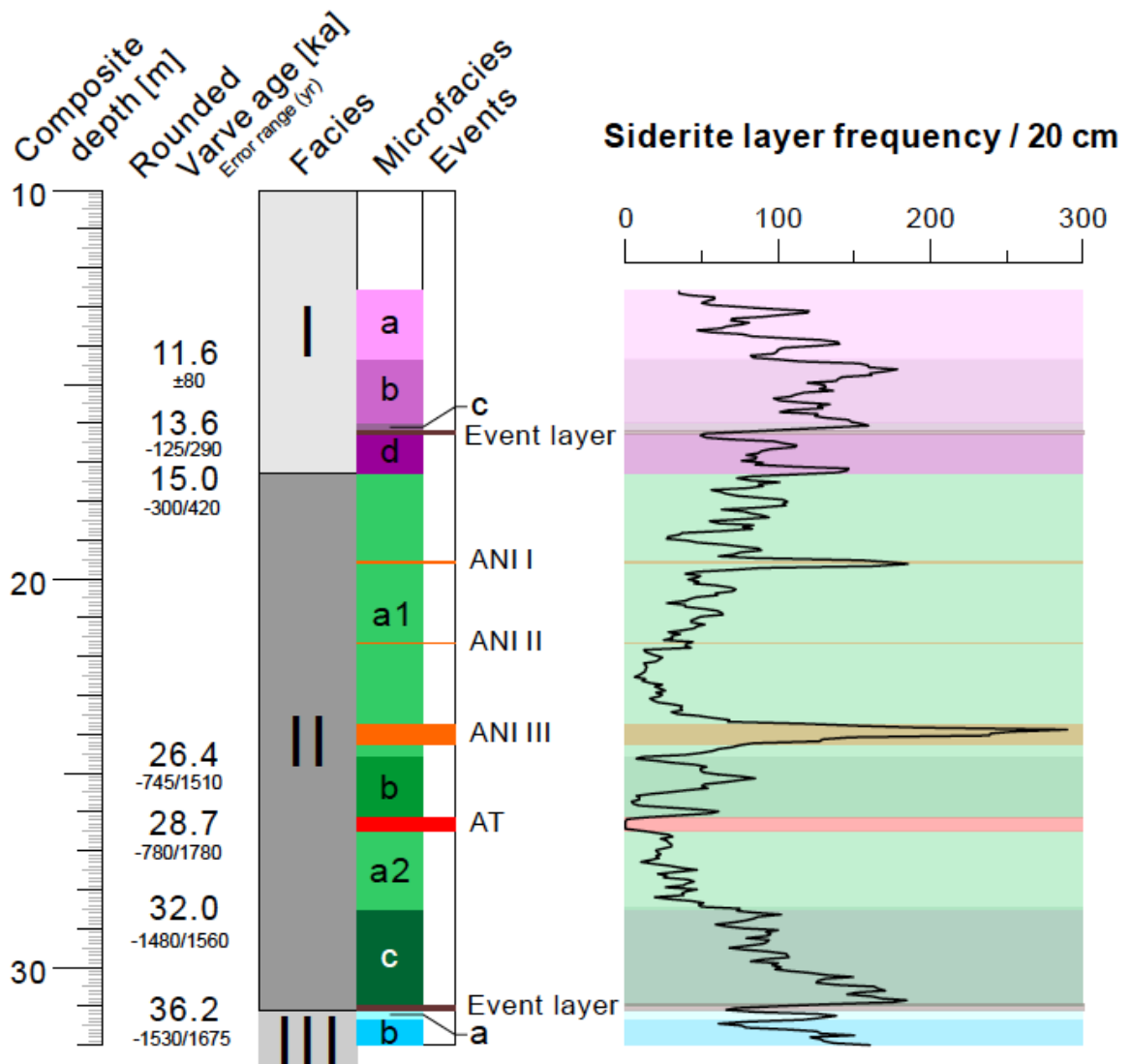
1280

1281

1282

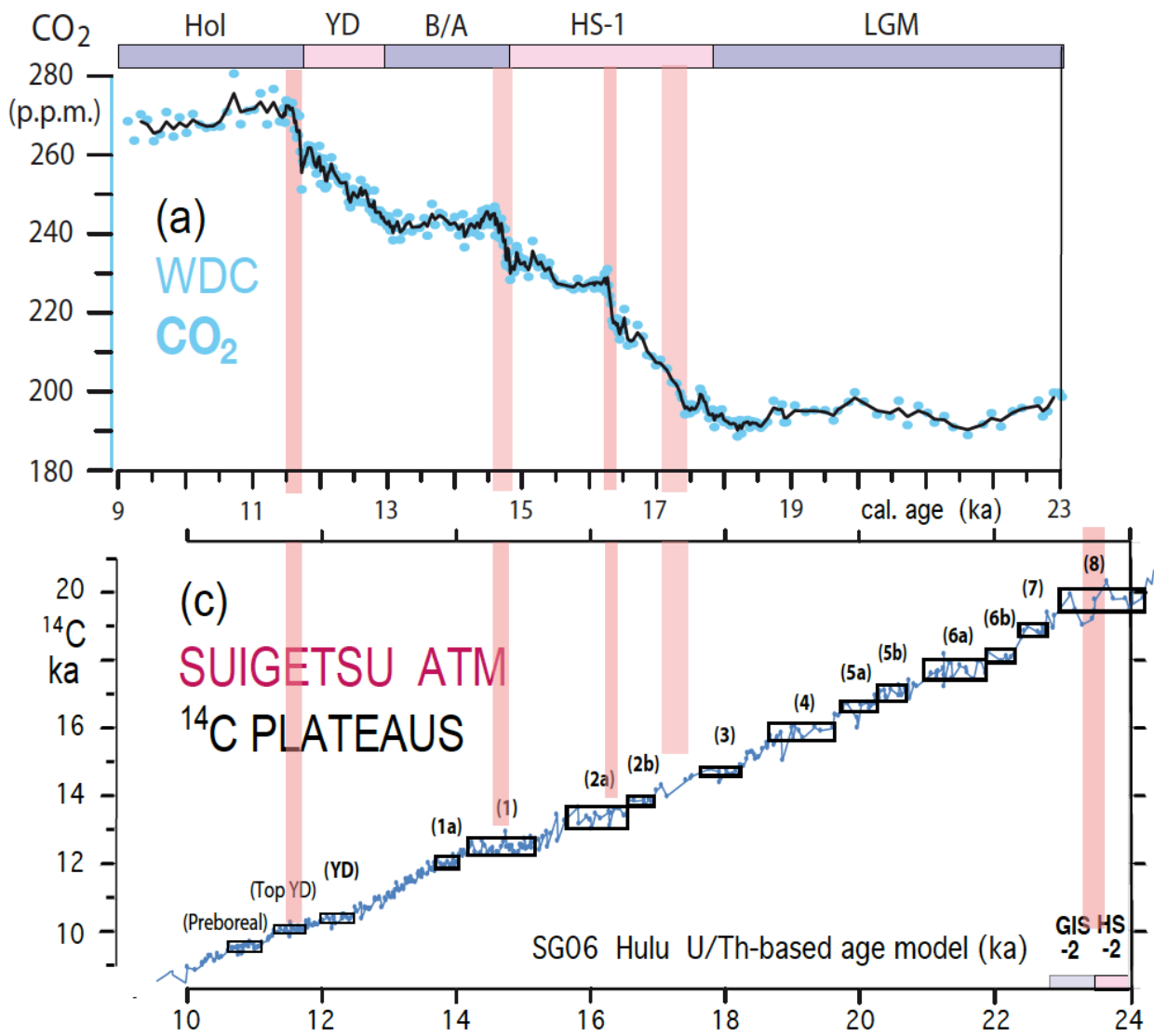
1283

1284 ✗ Fig. 5. Sediment facies and microfacies zones in Lake Suigetsu Core SG06, ~13–32
 1285 m depth (simplified and suppl. from Schlolaut et al., 2018). Microscopy-based frequency
 1286 of siderite layers with quality level 1–3 (= running average of layer counts per 20 cm
 1287 thick sediment section) serves as measure of seasonal lamination quality and shows
 1288 gradual transitions between varved and poorly varved sediment sections. Rounded
 1289 varve ages are microscopy based and constrain age of major facies and microfacies
 1290 boundaries. ANI I to ANI III mark core sections with ultrafine lamination due to
 1291 sedimentation rate minima, AT marks tephra layer named AT, ‘Event layers’ label major
 1292 thin mud slides probably earth quake-induced.s



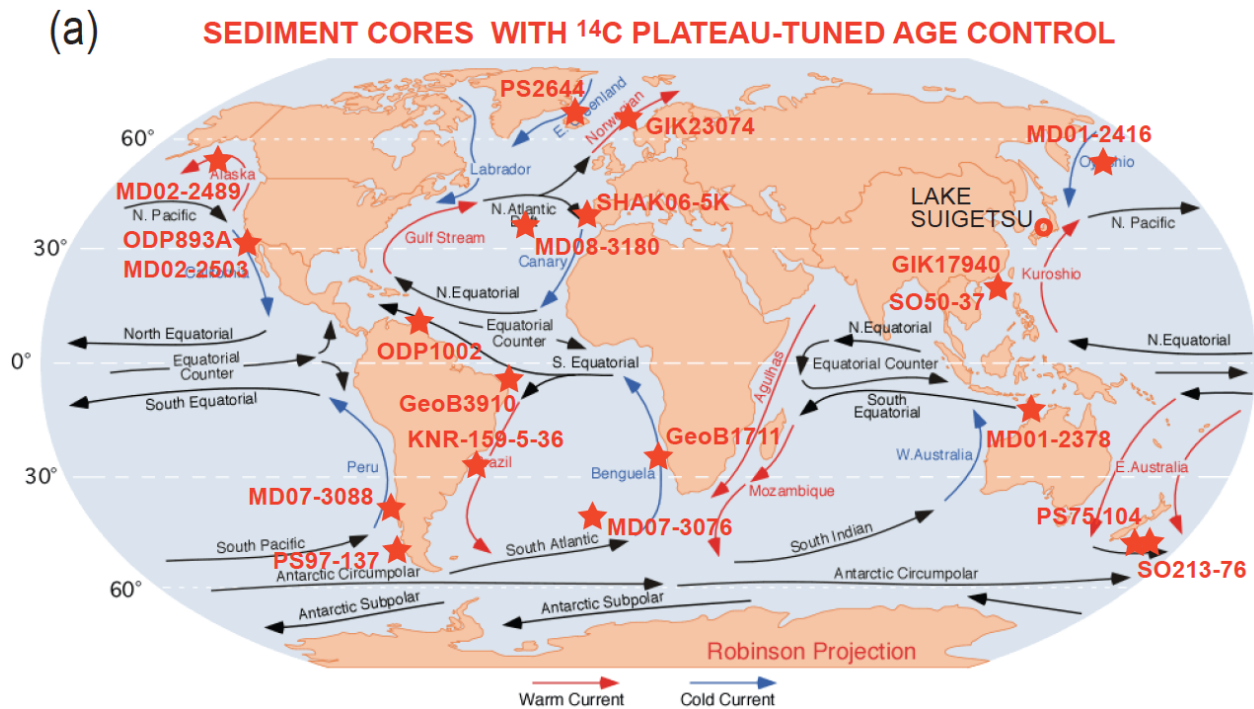
1293

1294 ✖ Fig. 6 (a). Four sudden steps (pink bars) in the deglacial atmospheric CO₂ rise at
 1295 West Antarctic Ice Sheet Divide ice core (WDC) reflect events of fast ocean degassing,
 1296 that may have contributed to the origin of deglacial ¹⁴C plateaus. Age control based on
 1297 ice cores (Marcott et al., 2014). (b) The steps are compared to suite of atmospheric ¹⁴C
 1298 plateaus dated by Hulu U/Th-based model ages (Bronk Ramsey et al., 2012). Hol =
 1299 Holocene; YD = Younger Dryas; B/A = Bølling-Allerød; HS = Heinrich stadials 1 and 2;
 1300 LGM = Last Glacial Maximum, GIS-2 = Greenland interstadial 2.
 1301

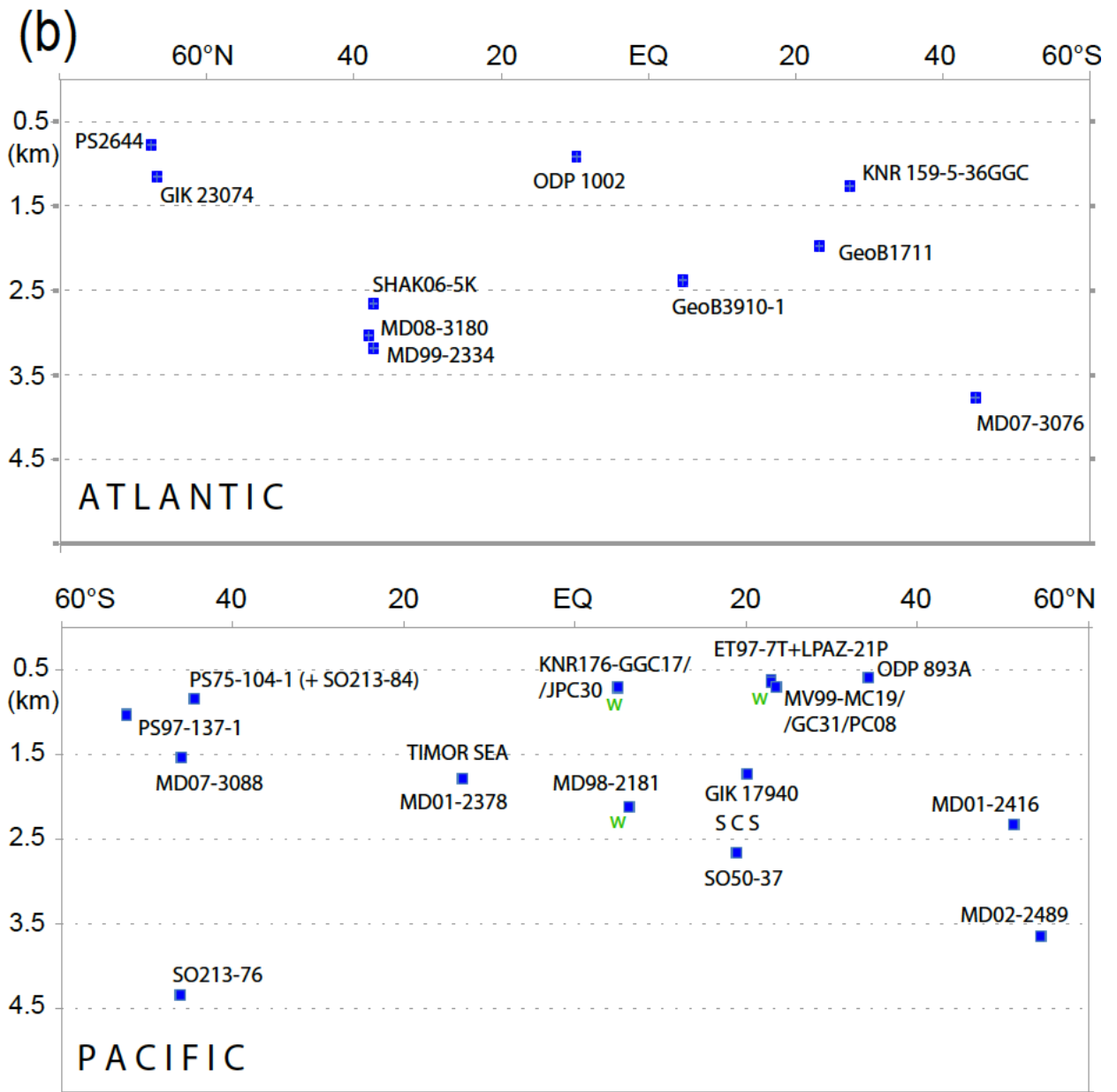


1302
 1303

1304 ✕ Fig. 7. Location (a) and water depth (km) (b) of sediment cores with age control based
 1305 on ^{14}C plateau tuning. ^{14}C reservoir ages of cores labeled with 'w' are derived from
 1306 samples with paired wood chunks and planktic foraminifers.



1307



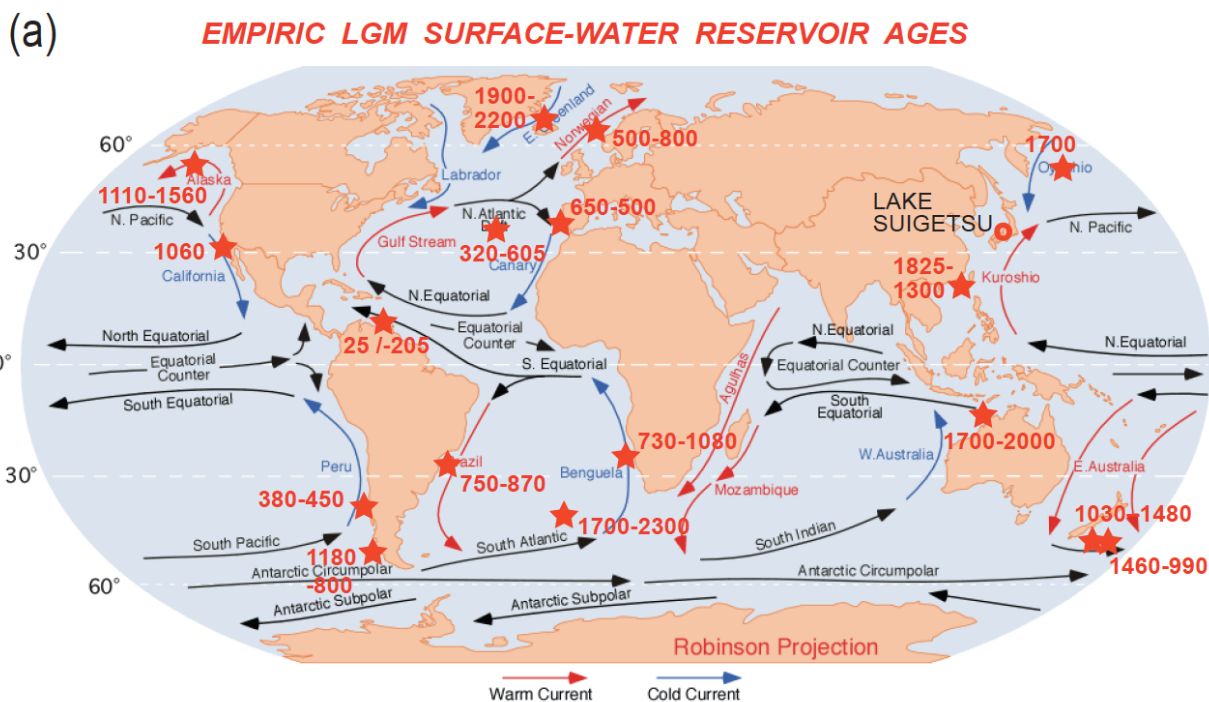
1308

1309

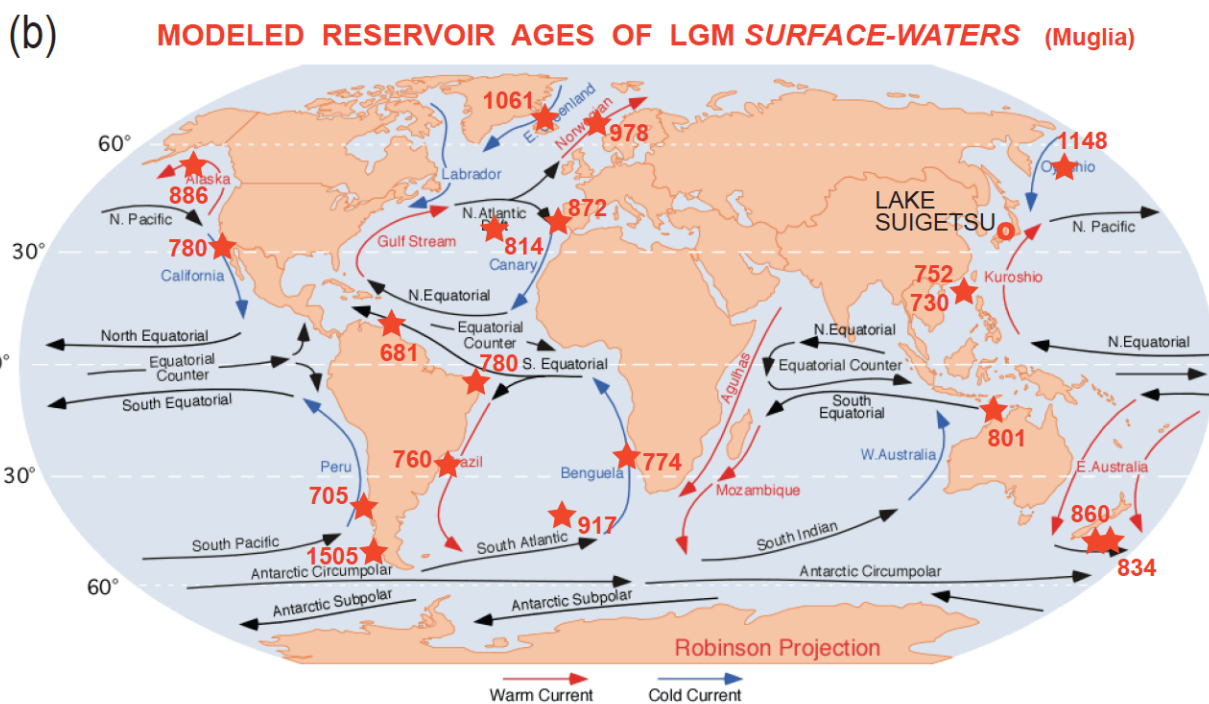
1310 √ Fig. 8. Global distribution of ^{14}C reservoir ages of Late LGM surface waters estimated
 1311 (a) by means of ^{14}C plateau tuning of planktic ^{14}C records. (b) Model-based estimates
 1312 (GCM of Muglia et al., 2018, assuming an AMOC strength of 13 Sv) for sites with
 1313 planktic foraminifera-based age values. X-Y graph (c) and map (d) show (rounded)
 1314 differences between observed and modeled values and their intra-LGM trends. Minor
 1315 differences are displayed in magenta, larger differences of >400 yr in red. Planktic
 1316 habitat depths and model estimates are largely confined to 0–100 m water depth.

1317 Arrows of surface currents delineate different sea regions important to assess potential
 1318 limits of spatial extrapolation of reservoir ages. Distribution of core numbers and
 1319 references for ¹⁴C records are given in Table 3a-c and Fig. 7a.

Fig. 8a

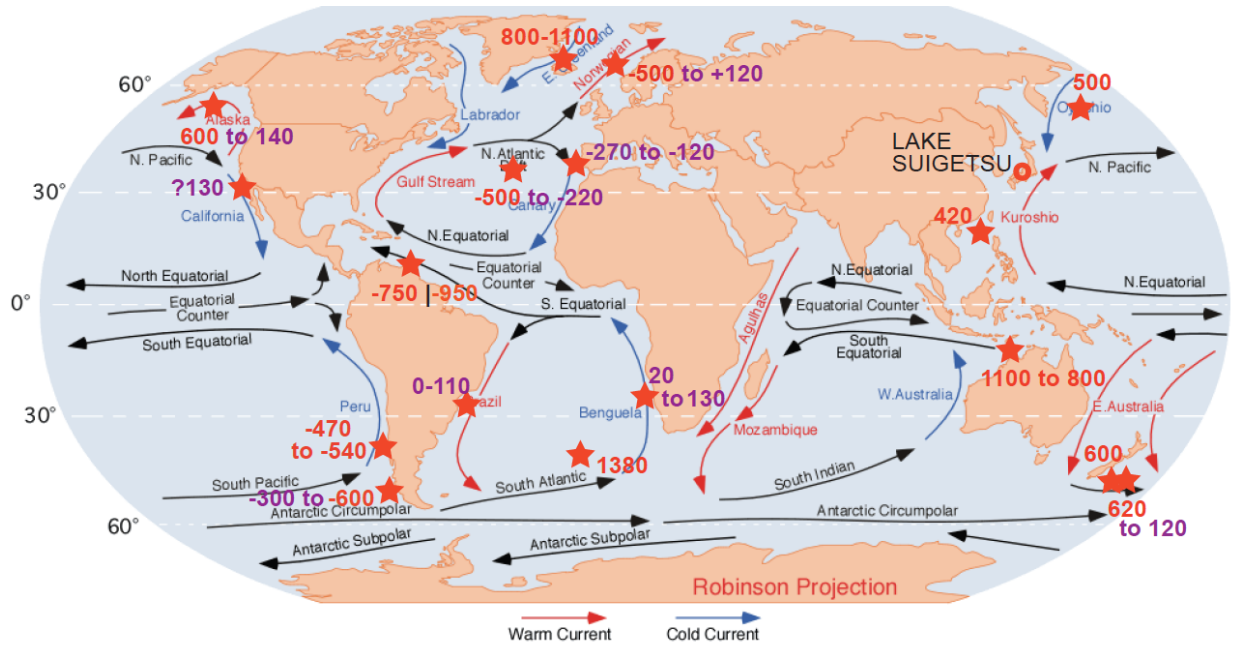


1320



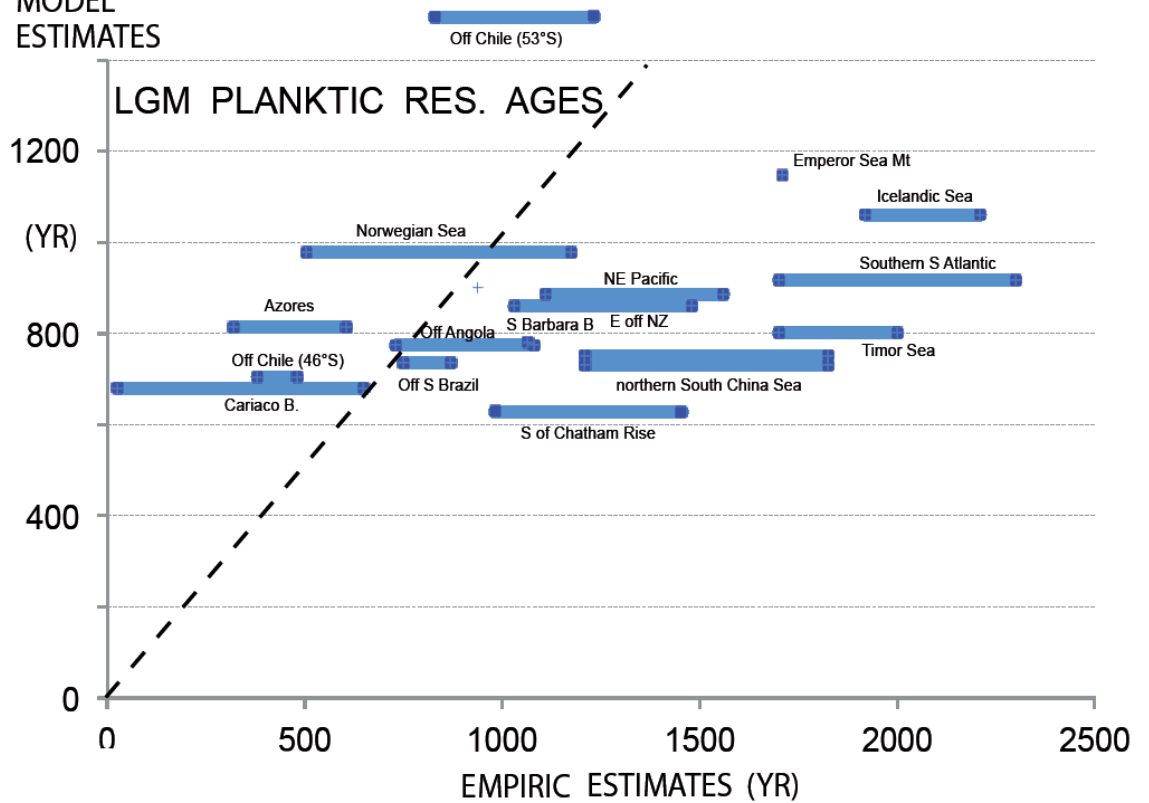
1321

(c) **EMPIRIC minus Muglia MODEL RESERVOIR AGES (yr) of LGM S.W.**



1322

(d) **MODEL ESTIMATES**

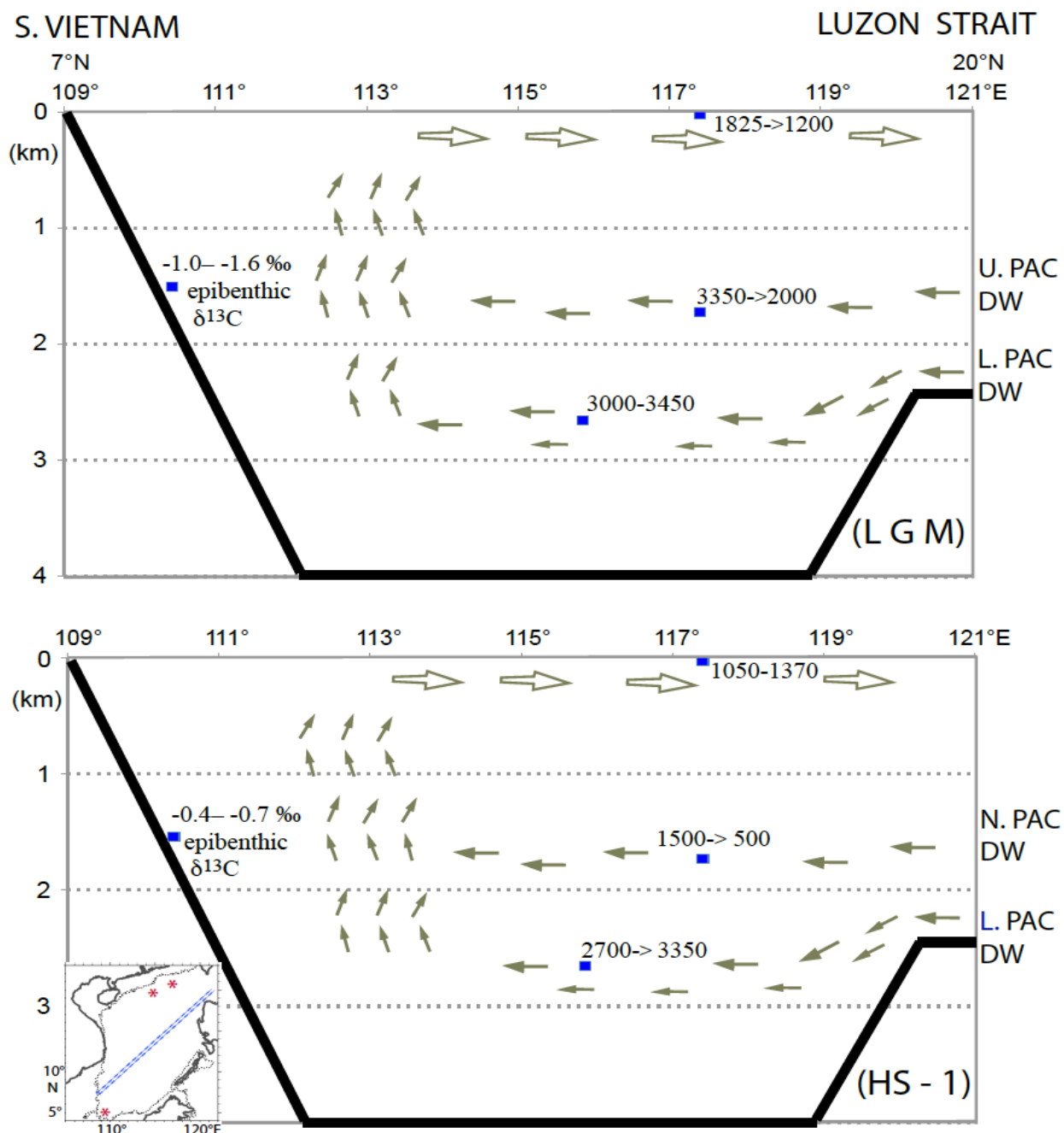


1323

1324

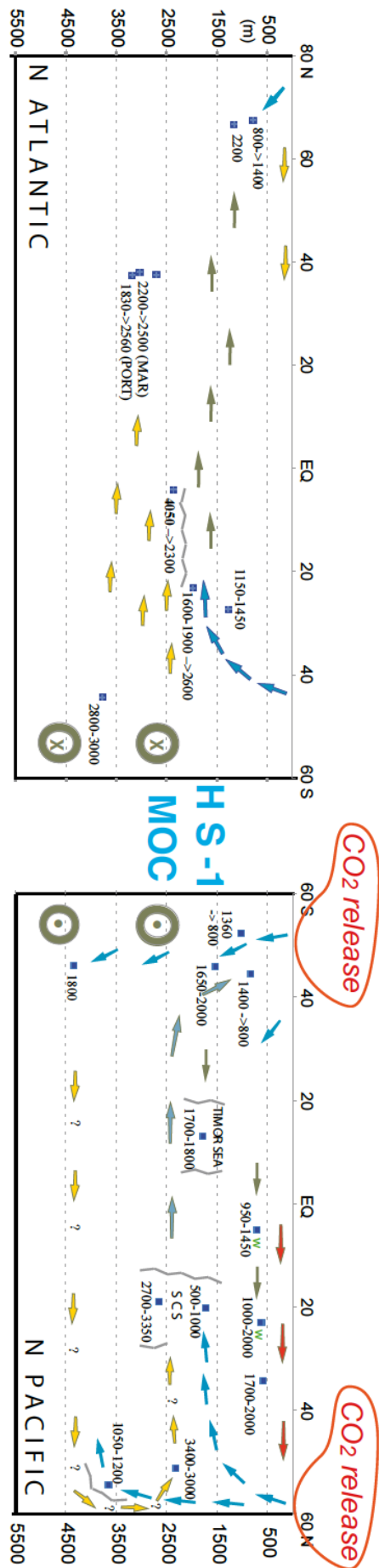
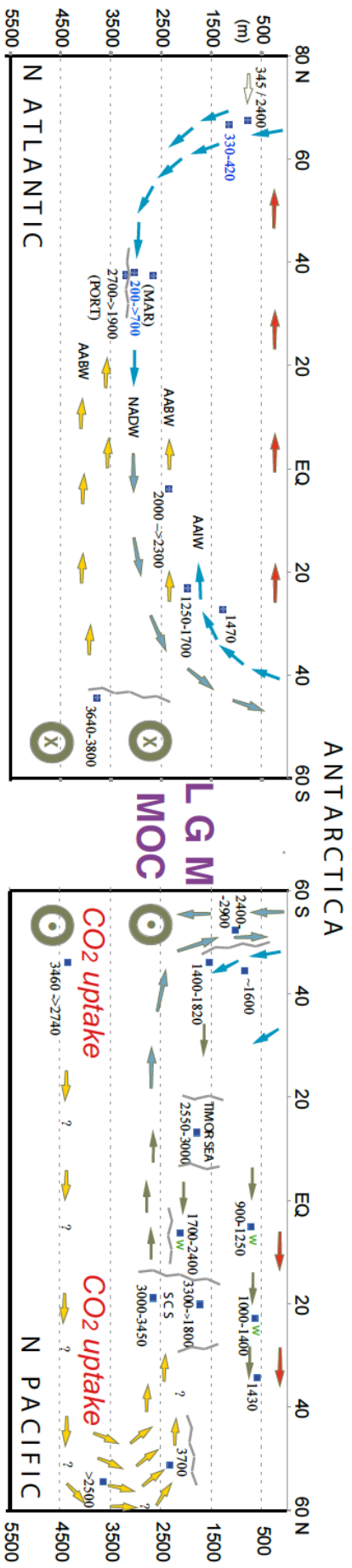
1325 √ Fig. 9. SW–NE transect of ^{14}C reservoir age and changes in ventilation age across
 1326 sites GIK17940 and SO50-37 in the South China Sea during late LGM (^{14}C Plateaus 5

1327 and 4; upper panel) and HS-1 (lower panel). Insert map shows location of transect and
 1328 core locations. Core locations are given in Fig. 7. An extreme epibenthic $\delta^{13}\text{C}$ minimum
 1329 in far southwest (Core GIK17964; Sarnthein et al., 1999) reflects an LGM incursion of
 1330 Lower/Upper Pacific Deep Waters (L./ U. PAC DW) with extremely high ^{14}C ventilation
 1331 age and DIC enrichment in contrast to a low ventilation age of North Pacific Deep Water
 1332 (N. PAC DW). Arrows show direction of potential deep and intermediate-water currents.



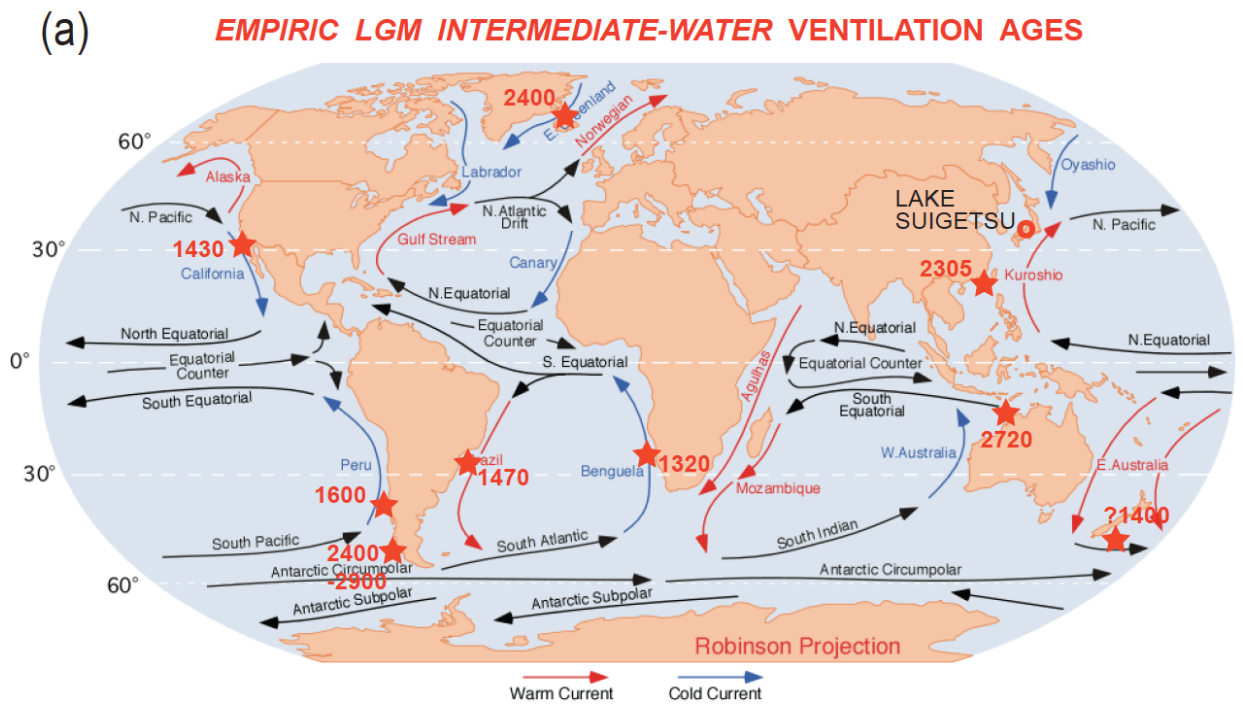
1333

1334 ✗ Fig. 10. 2D transects of the geometries of global ocean MOC. Arrows (blue = high,
1335 yellow = poor ventilation) suggest average deep and intermediate-water currents that
1336 follow the gradient from low to high benthic ventilation ages based on paired planktic
1337 ¹⁴C reservoir ages derived by means of ¹⁴C plateau tuning technique (Sarnthein et al.,
1338 2013, Balmer et al., 2018, Küssner et al., 2020, *subm.*). At some Pacific sites reservoir
1339 ages are based on paired ¹⁴C ages of planktic foraminifera and wood chunks (marked
1340 by green 'w'; Sarnthein et al., 2015; Zhao and Keigwin, 2018, Rafter et al., 2018). Red
1341 arrows suggest poleward warm surface water currents. Zigzag lines indicate major
1342 frontal systems separating counter rotating ocean currents (e.g., W of Portugal and N of
1343 MD07-307; after Skinner et al., 2014). (a) Late LGM circulation geometry (21–18.7 cal.
1344 ka), largely similar to today. Note the major east-west gradient of ventilation ages in the
1345 central North Atlantic, between Portugal (PORT) and Mid-Atlantic Ridge W of Azores
1346 (MAR). (b) HS-1 benthic ventilation ages reveal a short-lasting MOC reversal leading to
1347 Atlantic-style overturning in the subpolar North Pacific and coeval Pacific-style stratific-
1348 ation in the northern North Atlantic, with seesaw-style reversals of global MOC at the
1349 onset and end of early HS-1 (first proposed by Broecker et al., 1985, however, for LGM
1350 times). Increased ventilation ages reflect enhanced uptake of dissolved carbon in the
1351 LGM deep ocean (Sarnthein et al., 2013), major drops suggest major degassing of CO₂
1352 from both the deep Southern Ocean and North Pacific during early HS-1. – SCS =
1353 South China Sea. AABW = Antarctic Bottom Water; AAIW = Antarctic Intermediate
1354 Water. NADW = North Atlantic Deep Water. Small arrows within age numbers reflect
1355 temporal trends. Many arrows are speculative using circumstantial evidence of benthic
1356 δ¹³C records and local Coriolis forcing at high-latitude sites per analogy to modern
1357 scenarios. Location of sediment cores are given in Fig. 7, short-term variations in
1358 planktic and benthic ¹⁴C reservoir/ventilation age in Suppl. Fig. S2 and Table 3.

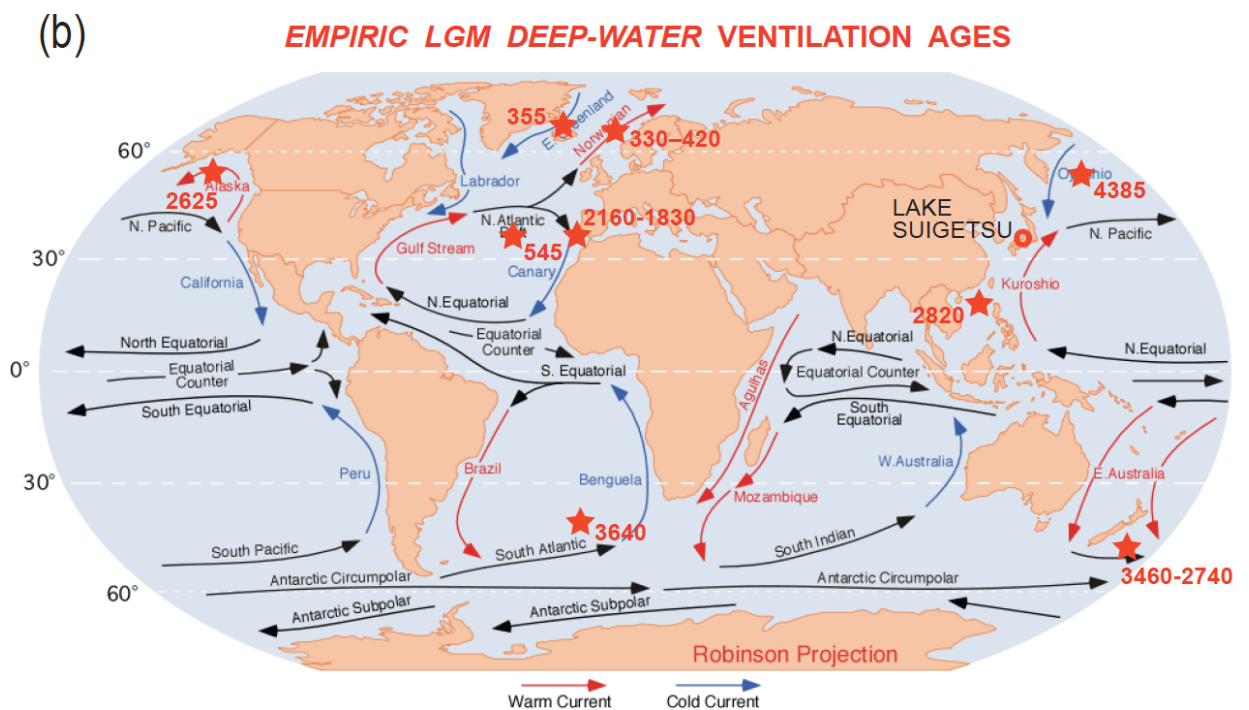


1360

1361 √ Fig. 11. Global distribution of ^{14}C reservoir ages obtained (a) for late LGM
1362 intermediate waters (100–1800 m w.d.) and (b) for LGM deep waters (>1800 m w.d.),
1363 including Site GIK 23074 at 1157 m in the Norwegian Sea).



1364



1365